Bony Abnormalities in Feline Models of GM2 Gangliosidosis

by

Patricia Michelle Beadlescomb

A thesis submitted to the Graduate Faculty of
Auburn University
in partial fulfillment of the
requirements for the Degree
of Master of Science

Auburn, Alabama
August 2, 2014

Key Words: GM2 Gangliosidosis, Tay-Sachs, Sandhoff, Bony Abnormalities, Computed Tomography

Approved by

Douglas R. Martin, Chair, Associate Professor, Department of Anatomy, Physiology, and Pharmacology; Scott-Ritchey Research Center
Nancy R. Cox, Professor and Director, Scott-Ritchey Research Center
Ronald D. Montgomery, Bruce Pratt Professor of Orthopedic Surgery, Department of Clinical Sciences
Dewey R. Wilhite, Instructor, Department of Anatomy, Physiology, and Pharmacology

Abstract

This study seeks to explore and quantify bony deformities in feline models affected with GM2 gangliosidosis with emphasis on long bones and cervical vertebrae, based on previous diagnostics exhibiting cervical spinal cord compression, luxating coxofemoral and patellar joints, and tibial bowing. We hypothesized that vertebral and long limb abnormalities initiate spinal cord compression and limb weakness, respectively. The study design was comprised of GM2 cats treated intracranially via adeno-associated virus (AAV) gene-therapy by thalami and intracerebroventricular (ICV) injections, GM2 untreated, and sex and age-matched normal and carrier cats. Whole body computed tomography (CT) scans were performed on GM2 affected and normal subjects. Scans were analyzed using Mimics Materialise Software and limb bones were printed using a 3D printer to obtain length measurements. Limb samples were sent to Louisiana State University for micro-CT analysis, and results were consistent with conventional CT findings. Significant differences were found in nearly all bone measurements, suggesting that bony abnormalities contribute to limb weaknesses. Vertebral column deformities did not reach significance, though spinal cord compression is clearly seen at necropsy in some animals. Future studies will be conducted to test alleviation of peripheral disease manifestations such as bony abnormalities.

Acknowledgements

"For I know the plans I have for you," declares the Lord, "plans to prosper you and not to harm you, plans to give you a hope and a future." Jeremiah 29:11 All of my life's work is done for God. Through Him, I have achieved success and Him alone. It is because of God that I have had this extraordinary opportunity to be involved in research at Scott-Ritchey. Thank you to all of Scott-Ritchey personnel, especially my mentor Dr. Martin who went against the odds and invited me into his lab.

Thank you to my committee member Drs. Nancy Cox, R.D. Montgomery, and Ray Wilhite for your endless assistance and guidance through this process.

I would be remiss if I didn't thank my wonderful parents. Thank you to my dad for believing in me, and always telling me that I can be anything that I want to be just as long as what I do makes me happy. Thank you to my mom for being my rock, listening to my sorrows and triumphs, and for always keeping me on my toes, because hard work=success.

A special thank you goes the Auburn University College of Veterinary Medicine Radiology Department. Without your cooperation this project would not have been possible.

Thank you to the NIH, NTSAD, and private donors for funding this study. Again, without your support this would not have been possible.

"God is within her, She will not fail" Psalm 46:5.

Table of Contents

Abstract……..……ii

Acknowledgements..…….....iii

List of Figures.....vi

List of Tables.....viii

Chapter 1: Introduction

a. GM2 Gangliosidosis.....1

b. Gene Therapy.....4

c. Specific Problem.....5

d. Study Objectives.....6

Chapter 2: Materials, Methods, and Literature Review

a. Computed Tomography.....7

b. Mimics, 3ds Max, and 3D Printing.....8

d. Literature Review.....14

Chapter 3: Bony Abnormalities in Cats with Sandhoff Disease

a. Results.....18

b. Discussion.....42

c. Application in Veterinary and Human Medicine.....46

Chapter 4: Summary

a. Summary.....47

b. Conclusions.....48

c. Limitations.....49

d. Future Research Paths.....49

References.....51

Appendix.....53

μCT Definitions.....64

List of Figures

Figure 1. Human ganglioside pathway.....3

Figure 2. 3D dorsal view of axial skeleton.....9

Figure 3. 3D left lateral view of axial skeleton.....9

Figure 4. Representation of long bone measurements.....10

Figure 5. 3D cranial view of left femur.....11

Figure 6. 3D medial view of left femur.....11

Figure 7. Representation of ventral length measurement.....12

Figure 8. Representation of canal space measurement.....13

Figure 9A. C1 canal space.....21

Figure 9B. C2 canal space.....21

Figure 10A. C1 ventral length.....22

Figure 10B. C2 ventral length.....22

Figure 11A. T1 canal space.....23

Figure 11B. T2 canal space.....24

Figure 12A. T1 ventral length.....24

Figure 12B. T2 ventral length.....25

Figure 13A. L1 canal space.....26

Figure 13B. L2 canal space.....26

Figure 14A. L1 ventral length.....27

Figure 14B. L2 ventral length.....27

Figure 15A. C1/C2 compression site.....30

Figure 15B. T1/T2 compression site.....30
Figure 15C. L1/L2 compression site.....31
Figure 16A. Average left femoral length.....33
Figure 16B. Average right femoral length.....33
Figure 17A. Average left tibial length.....35
Figure 17B. Average right tibial length.....35
Figure 18A. Average left humeral length.....37
Figure 18B. Average right humeral length.....37
Figure 19A. Average left ulnar length.....40
Figure 19B. Average right ulnar length.....40
Figure 19C. Average left radial length.....41
Figure 19D. Average right radial length.....41
Figure 20A. 3D reconstructed skeleton.....43
Figure 20B. 3D reconstructed skeleton.....43
Figure A1. 3D reconstruction of µCT image of mature distal femora.....55
Figure A2. 3D reconstruction of µCT mature images.....56
Figure A3. 3D reconstruction of µCT images of immature distal femora.....60
Figure A4. 3D reconstruction of µCT immature images.....61

List of Tables

Table 1. Cats in bony abnormality study.....7

Table 2A. Vertebral measurements.....19

Table 2B. Vertebral measurements.....20

Table 3. Spinal cord compression site.....29

Table 4. Femur measurements.....32

Table 5. Tibia measurements.....34

Table 6. Humerus measurements.....36

Table 7. Ulna measurements.....38

Table 8. Radius measurements.....39

Table A1.A µ-CT measurements.....57

Table A1.B µ-CT measurements.....58

Chapter 1

Introduction

GM2 Gangliosidosis

Lysosomal storage diseases (LSD) are caused by a deficient enzyme needed to facilitate the lysosome in catabolizing molecular waste products and occur globally in 1:5000 human live births (Fuller *et al*, 2006) with 1:40,000 reported in the USA (Martiniuk *et al*, 1998) alone. The inability to properly eliminate molecular waste leads to storage material accumulation within all cells resulting in cell toxicity and eventually death. GM2 gangliosidosis (GM2) is a rare autosomal recessive disease that originally plagued people of Jewish descent but is now found more commonly in the general population. GM2 can affect all age ranges including infants (Bley *et al*, 2011), juveniles (Maegawa *et al*, 2006), and adults (Federico *et al*, 1991). Infants with GM2 typically present with clinical signs by 5 months of age and reach mortality at 3 to 5 years of age (Bley *et al*, 2011). Juveniles present a subacute disease progression with clinical onset from 1.5 to 15 years of age, reaching mortality at an average of 19 years (Maegawa *et al*, 2006). Finally, the adult onset of GM2 varies widely in age of clinical signs from 10 to 30 years of age, and these patients can live into their seventh or eighth decade (Federico *et al*, 1991).

GM2 is classified into 3 variants, all of which are deficient in the activity of a lysosomal hydrolase, β-N-acetylhexosaminidase (Hex; EC 3.2.1 52): Tay-Sachs Disease (TSD), Sandhoff disease (SD), and GM2 Activator (GM2A) deficiency. Hex consists of 2 primary isozymes HexA and Hex B. Hex A is comprised of an α and β-subunit, and Hex B is a homodimer of β-subunits.TSD is caused by an absence of the α subunit, creating a deficiency of Hex A. SD is

caused by a β subunit deficiency and results in the absence of both Hex A and Hex B. A deficiency of the GM2 activator protein prevents the formation of the GM2 ganglioside complex, required for Hex A to remove the terminal *N*-acetylgalactosamine residue of the molecule (Liu *et al*, 1997). Ganglioside degradation in normal humans is shown in Figure 1 (Sandhoff, 2013). GM2 carriers only express approximately 50% of the respective subunit but are phenotypically normal. For an individual to function properly without showing clinical signs, it is estimated that only approximately 10% of normal Hex activity is required.

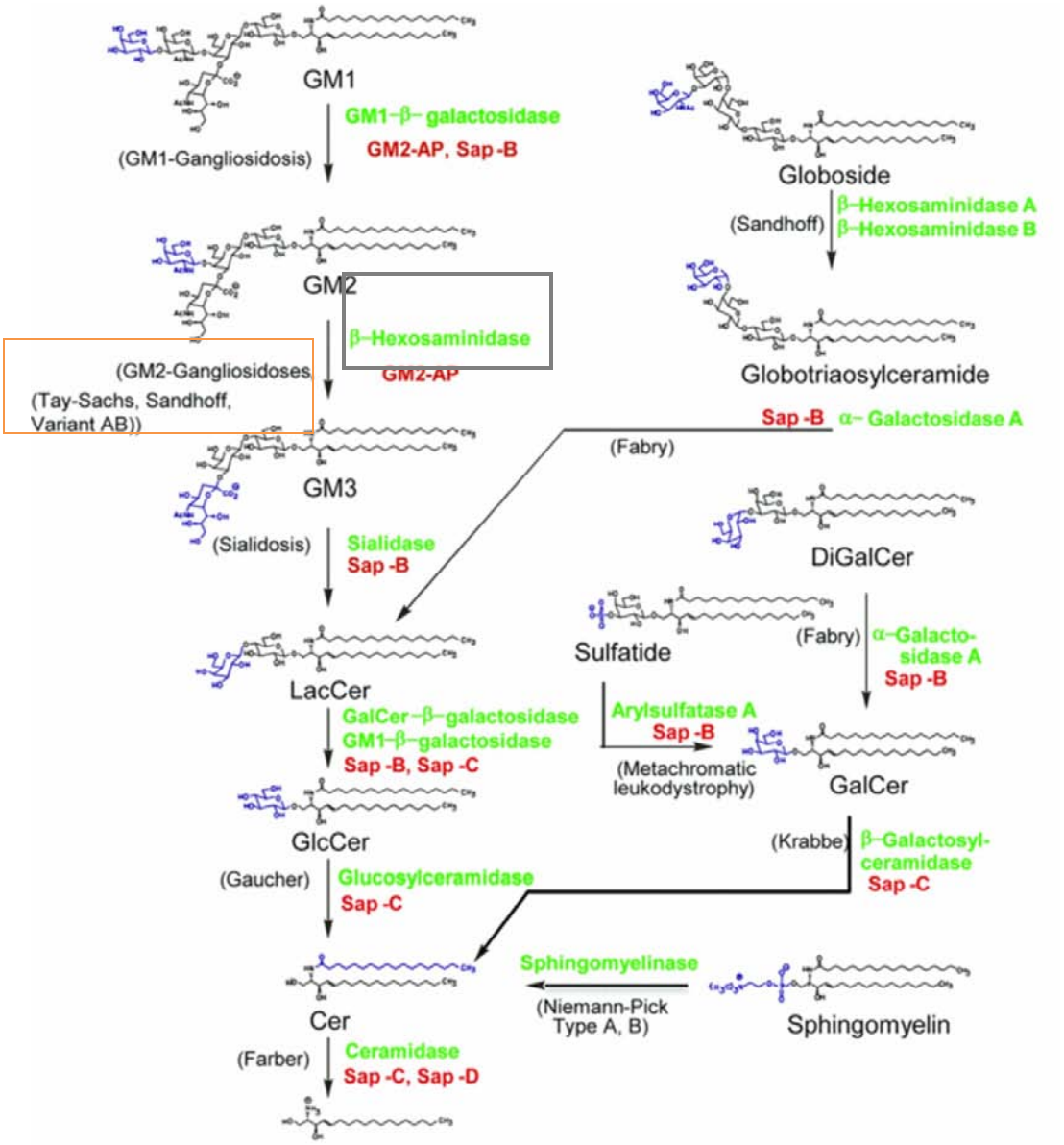

Figure 1: Human ganglioside pathway. Normal ganglioside catabolism occurs in the stepwise process visible in the diagram. Note that any deficiency in enzymes, such as mutation of β-hexosaminidase (outlined in grey), results in the specified storage diseases. Storage diseases of interest are outlined in orange. (Sandhoff, 2013). (monosialotetrahexosylganglioside (GM1); disialotetrahexosylganglioside (GM2); trisialotetrahexosylganglioside (GM3); lactosylceramide (LacCer); glucosylceramide (GlcCer); ceramide (Cer); galactosylceramide (GalCer); digalactosylceramide (DiGalCer); GM2 activator protein (GM2-AP); sphingolipid activator protein (SAP-B,C,D).

Gene Therapy

GM2 is currently incurable in both humans and animals. While treatments are being tested in animal models, only supportive care is available to human GM2 patients. Although several animal species have been used for GM2 research such as knockout mice (Sango *et al*, 1995), cats (SD) (Cork *et al*, 1978) and sheep (TSD) (Porter *et al*, 2011;Torres *et al*, 2010) are used as research models. Due to their similar brain to body size ratio when compared to humans (Vite *et al*, 2003), large animal models are important for developing human therapies. GM2 immature cats reach humane endpoint at approximately 4.5 months of age, with treated cats living over 4 times longer. Humane endpoint is defined by the inability to stand on 2 consecutive days. Untreated cats typically reach humane endpoint due to whole-body tremors that compromise their ability to stand. However, treated cats lose the ability to stand because of a progressive limb weakness (most prominent in pelvic limbs). Most treated cats never develop whole-body tremors; therefore, peripheral disease may trigger the humane endpoint before actual neurologic disease progression.

According to Bradbury *et al*, cats' brains are only 16 times smaller than a human infant's brain (compared to 1000 times smaller in mice); therefore, central nervous system (CNS) therapeutic delivery studies in cats are a good approximation of challenges to be expected in humans (Bradbury *et al*, 2009). Both cats and sheep are treated with gene-therapy intracranially via adeno-associated virus (AAV) vectors which have been used for over a decade in developing treatments of inherited disorders. AAV vectors are derived from DNA viruses in the family *Parvoviridae* (Berns, 1990). AAV are nonpathogenic, can infect non-dividing cells (such as

neurons), and are used only as a vehicle to transport needed genetic material into affected cells (Rabinowitz *et al*, 2000;Vite *et al*, 2003). Treatments consist of a single injection of AAV-gene therapy into brain targets, including thalamus (THAL), cisterna magna (CM), and/or deep cerebellar nuclei (DCN). Intracerebroventricular (ICV) delivery into the lateral ventricle is also commonly performed.

Specific Problem

A cohort of cats were treated via lateral ventricular and bilateral thalami injections (ICV-THAL) with AAVrh8 vectors expressing feline Hex α and β subunits in a 1:1 ratio. This cohort of cats was used in the skeletal deformity study for two primary reasons: 1. AAV treatment increased their lifespan and overall quality of life, living >4 times longer as compared to GM2 immature subjects; however, this increase in lifespan also resulted in peripheral disease manifestations not seen in untreated animals, including severe skeletal abnormalities. 2. Similar skeletal deformities in GM2 cats may be encountered in human clinical trials; therefore, quantification and physiological studies of bony abnormalities are needed in order to better understand how to manage them. However, all treated cats exhibit a progressive pelvic limb weakness across all treatment groups with an inconsistent yet sometimes severe thoracic limb weakness as well. Spinal cord compression is also of concern, possibly due to bony over-proliferation which is most severe in cervical vertebrae but may also be found in the thoracic and/or lumbar regions. Diagnostic imaging consisting of magnetic resonance imaging (MRI) and radiographs from previous experiments demonstrated compression of the spinal cord consistently at C2-C3, bony

deformities such as tibial bowing, abnormal development of vertebral bodies and smaller stature of GM2 cats compared to normal cats. It has long been hypothesized that bone density of GM2 cats is lower than normal cats, leading to bone brittleness and smaller stature. Although AAV-gene therapy has greatly reduced neurologic disease in cats, peripheral disease not previously observed in younger GM2 immature cats is becoming clinical. Clinical demonstration of peripheral disease typically results in the animal reaching humane endpoint due to overt limb weakness. Therefore, studies must be conducted to identify the underlying issue so that it may be resolved, ultimately leading to an overall increase in quality and length of life in both animal models and humans.

Study Objectives

- Observe gross differences in limb bones and vertebrae.
- Quantify differences in limb bones by measuring length of bone.
- Quantify differences in vertebral changes, specifically cervical vertebrae.
- Evaluate findings and correlate them to clinical signs, i.e., thoracic/pelvic limb weakness, spinal cord compression deficits, etc.

This study is organized into 4 chapters. Following the introductory Chapter One, Chapter Two details the methodology and contains a literature review of lysosomal storage diseases resulting in bony abnormalities. Chapter Three outlines the results from skeletal experiments as well as discussions of results. Lastly, Chapter Four states conclusions, explains limitations, and outlines future research plans.

Chapter 2

Materials, Methods, and Literature Review

Computed Tomography

Computed tomography (CT) scans were performed using a General Electric high-speed CT/*i* scanner with 1 millimeter (mm) slice thickness (Fairfield, CT). Cohorts consisted of the following: 4 GM2+AAV mature cats with 3 age and sex-matched controls (2 normal and 1 carrier; *carriers do not demonstrate any skeletal differences compared to normal*); and 3 GM2 immature cats with 2 normal control cats.

Table 1: Cats in bony abnormality study

Cat #	Treatment	Treatment Age (Months)	Gender	Genotype	Age at Endpoint (Months)
7-1010	Untreated	n/a	Female	GM2	5.0
7-1006	Untreated	n/a	Female	GM2	5.0
7-1057	Untreated	n/a	Female	GM2	4.1
11-1015	Immature Control	n/a	Female	Normal	5.0
11-1030	Immature Control	n/a	Female	Normal	ongoing
11-900	ICV-THAL	0.9	Female	GM2	30.8
7-943	ICV-THAL	1.1	Male	GM2	23.7
7-945	ICV-THAL	1.1	Female	GM2	17
7-979	ICV-THAL	1.3	Male	GM2	21.3
8-1670	Mature Control	n/a	Male	Normal	ongoing
100B-909	Mature Control	n/a	Female	Normal	ongoing
100B-914	Mature Control	n/a	Male	GM2A Carrier	ongoing
9-1594	Mature Control	n/a	Female	GM1 Carrier	29.7

Table 1: ICV-THAL (intracerebroventricular and bilateral thalami single injection with AAV-gene therapy). Most normal control cats are still ongoing in other studies.

Animals were sedated with intramuscular injections of dexmedetomidine (0.5 micrograms (µg)/milliliters (mL) and ketamine (100µg/mL) and scanned under general anesthesia using

isoflurane (0.5-2%) for approximately one hour. To do full body scans, the scanner was allowed time to cool between scans, resulting in several overlapping segments per cat, accounting for the increased scan time compared to usual CT scans. Multiple scans per cat did not adversely affect data collection and analyses.

Mimics, 3ds Max, and 3D Printing

Mimics 3 dimensional (3D) imaging software (Materialise, Plymouth, MI) was used as the primary imaging software to reconstruct and quantify bony differences between GM2 and normal cats. In Mimics, the default bone threshold was selected to reconstruct entire skeletons. After the full skeleton was reconstructed, overall morphology was observed. Secondly, full skeletons were separated into axial (figures 2 and 3) and appendicular (figure 5 and 6) skeletal sections.

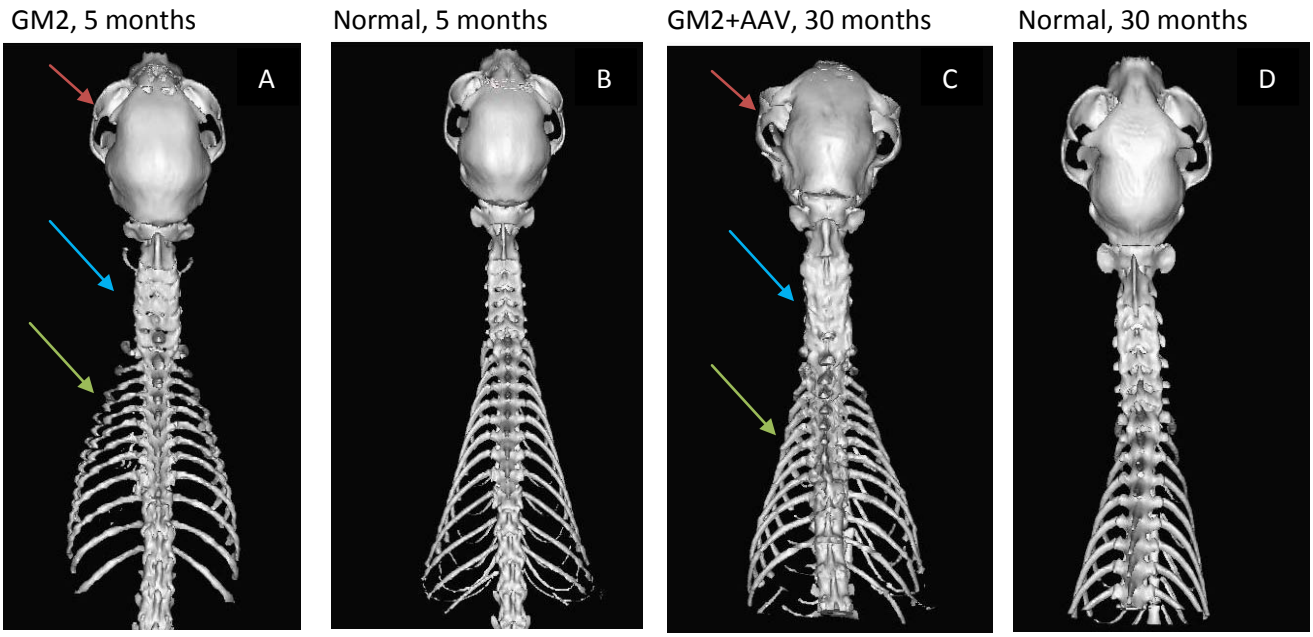

Figure 2: 3D dorsal view of axial skeleton. Note: The presence of both GM2 untreated and treated cats' misshapen cervical vertebrae (blue arrow) with *bony bridging*, malformed thoracic cage (green arrow), and dysmorphic skull (red arrow) as compared to sex/age-matched control.

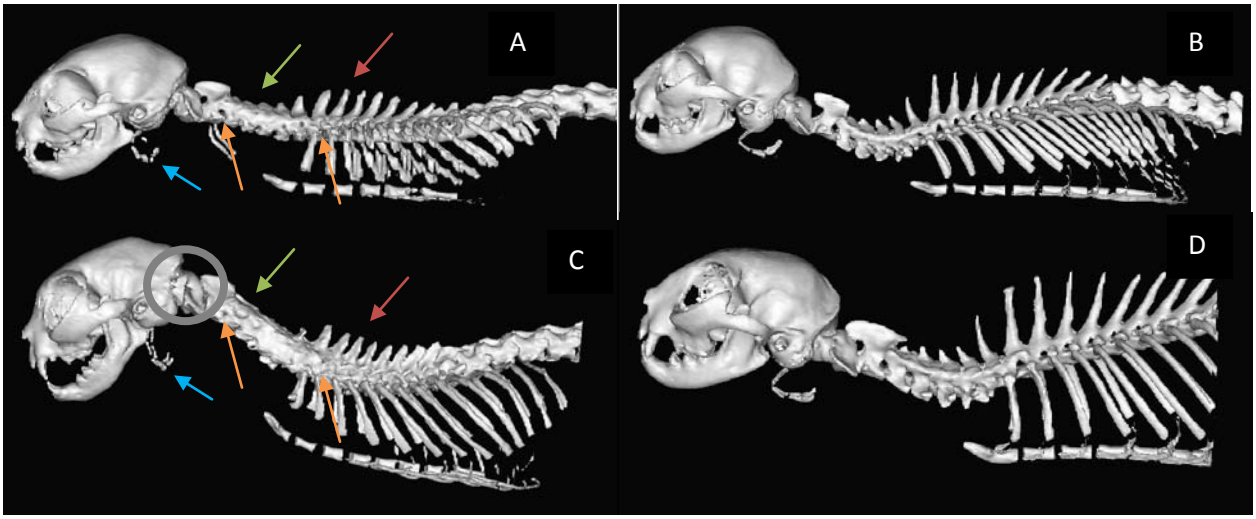

Figure 3. 3D left lateral view of axial skeleton. A-D Same subjects as Figure 2. Note malformed hyoid processes (blue arrow), fusion of cervical vertebrae with an absence of visible spinous processes (green arrow), stunting of spinous processes of thoracic vertebrae (red arrow), and inability to discern intervertebral foramen (orange arrow) of both GM2 untreated and treated cats compared to sex/age-matched normal control. Note the degree of extension in the neck is limited in C as compared to D (grey circle).

Lastly, limb long bones were isolated individually with radius/ulna and tibia/fibula remaining intact for measurements. Length measurements were obtained on each isolated bone(s) using the "measure distance tool" within Mimics. Additionally, isolated bone files were sent to the Auburn University College of Veterinary Medicine (AUCVM) radiology department for 3D printing, Makerbot Replicator 2 (Brooklyn, NY). Length measurements of 3D prints were measured using General 6 inch calipers (New York City, NY; Figure 4). Bone measurements were taken as the absolute length.

Figure 4: Representation of long bone measurements. Left: Humerus. Right: Femur. All long bones were 3D printed and measured in mm using calipers.

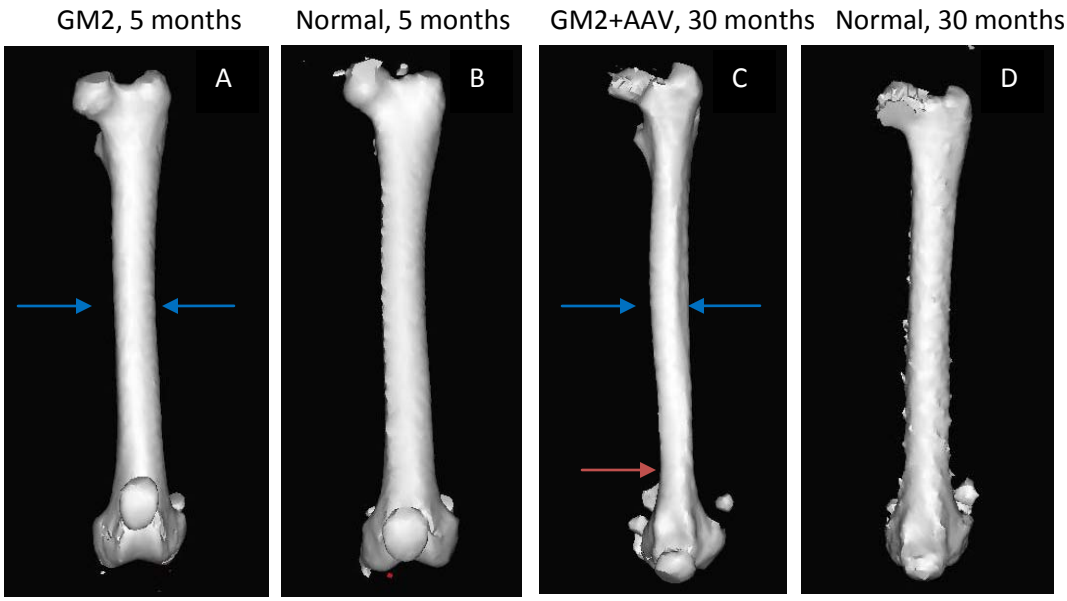

Figure 5. 3D cranial view of left femur. Note femurs are scaled to size for viewing.. A&B: Note overall normal morphology of GM2 cat compared to normal (blue arrows). C&D: Note irregularly shaped femoral shaft with narrowing at distal end (red arrows) in GM2+AAV cat. D: irregular appearance of bone shaft is due to CT artifact.

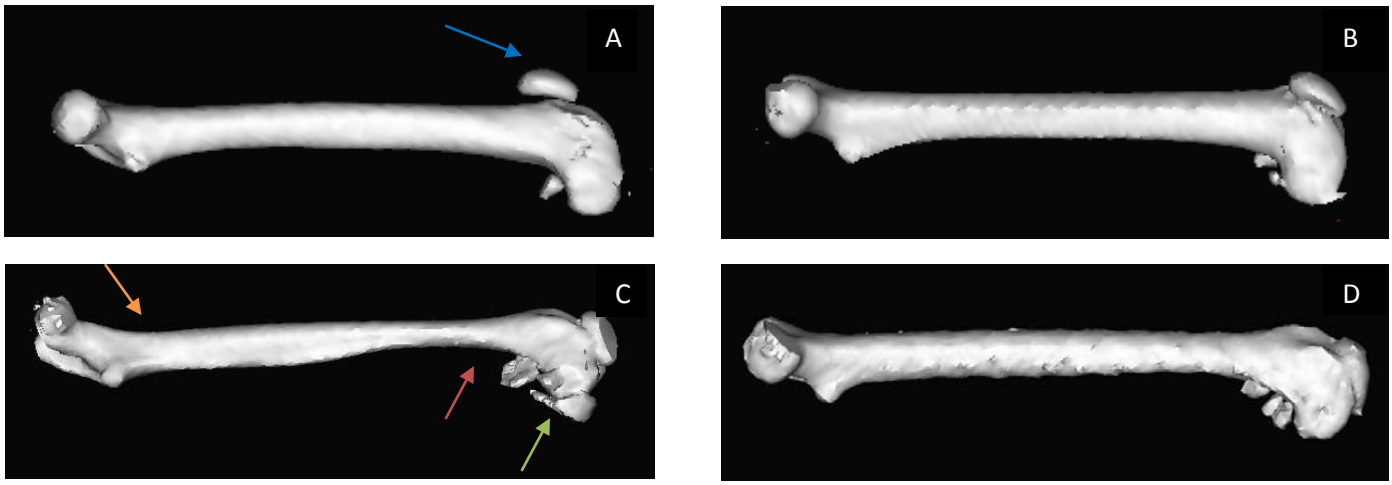

Figure 6. 3D medial view of left femur. Note femurs are scaled to size for viewing. A. GM2 immature female at 5 months. B. Normal female at 5 months. C. GM2+AAV female at 30 months. D. Carrier female at 30 months. Note deviated patella in untreated cat compared to normal control (blue arrows). Comparing C &D, note narrowing of distal femoral shaft (red arrows), significant growth of an osteophyte on the medial condyle (green arrows), and a "twisting" appearance of proximal femoral shaft (orange arrows).

Finally, vertebral measurements (figures 7 and 8) were obtained within Mimics in a sagittal plane using the same distance "measuring tool" by placing the cross bar on the most lateral aspects of the vertebral canal space. Also measured in a sagittal plane were C1, C2, T1, T2, L1, and L2 ventral vertebral bone lengths, canal space (the space in which the spinal cord lies); measured from dorsal to ventral, and spinal cord reconstructions. Various Mimics files were imported into Autodesk 3ds Max (San Rafael, CA) to be rendered together if separated by CT scans and/or to generate 3D printed visual aids of entire cat skeletons. No measurements were conducted within 3ds Max software. Bones were analyzed for statistics using a 1-tailed t-test and considered significantly different if p-value ≤ 0.05 (Zar, 1984).

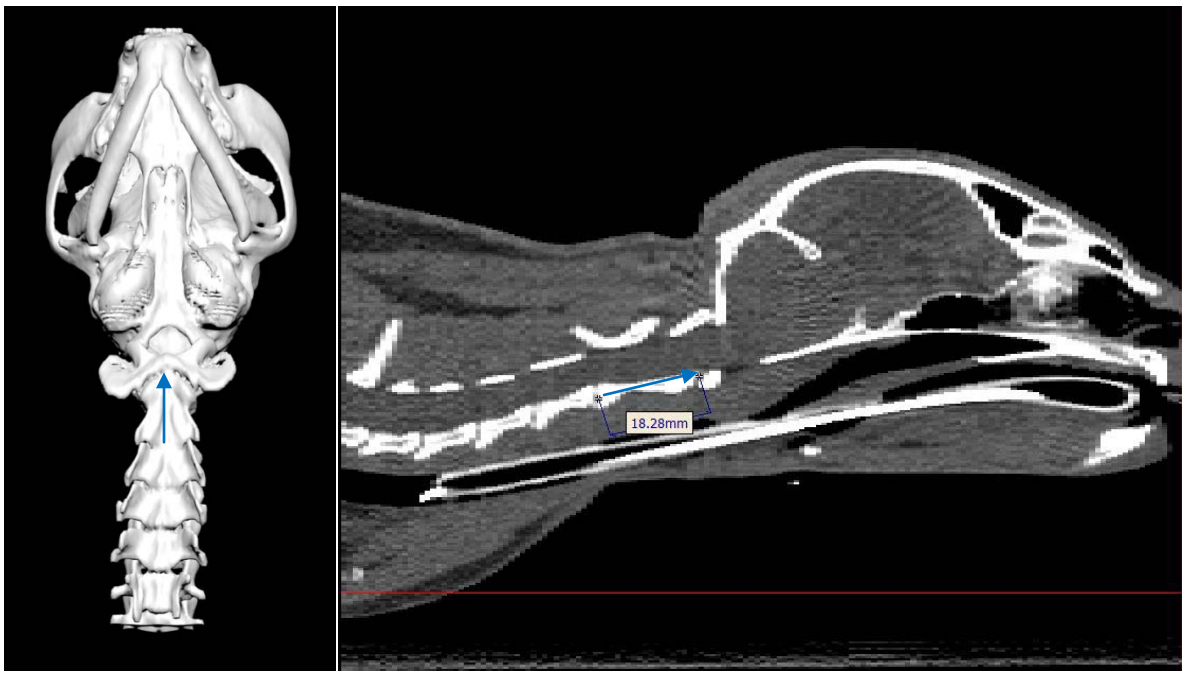

Figure 7: Representation of ventral length measurement. Left: Disarticulated reconstruction of partial axial skeleton. Right: Actual measurement conducted within Mimics software. Measurements (mm) were conducted from cranial to caudal on ventral vertebral bodies. Blue arrows indicate area of measurement.

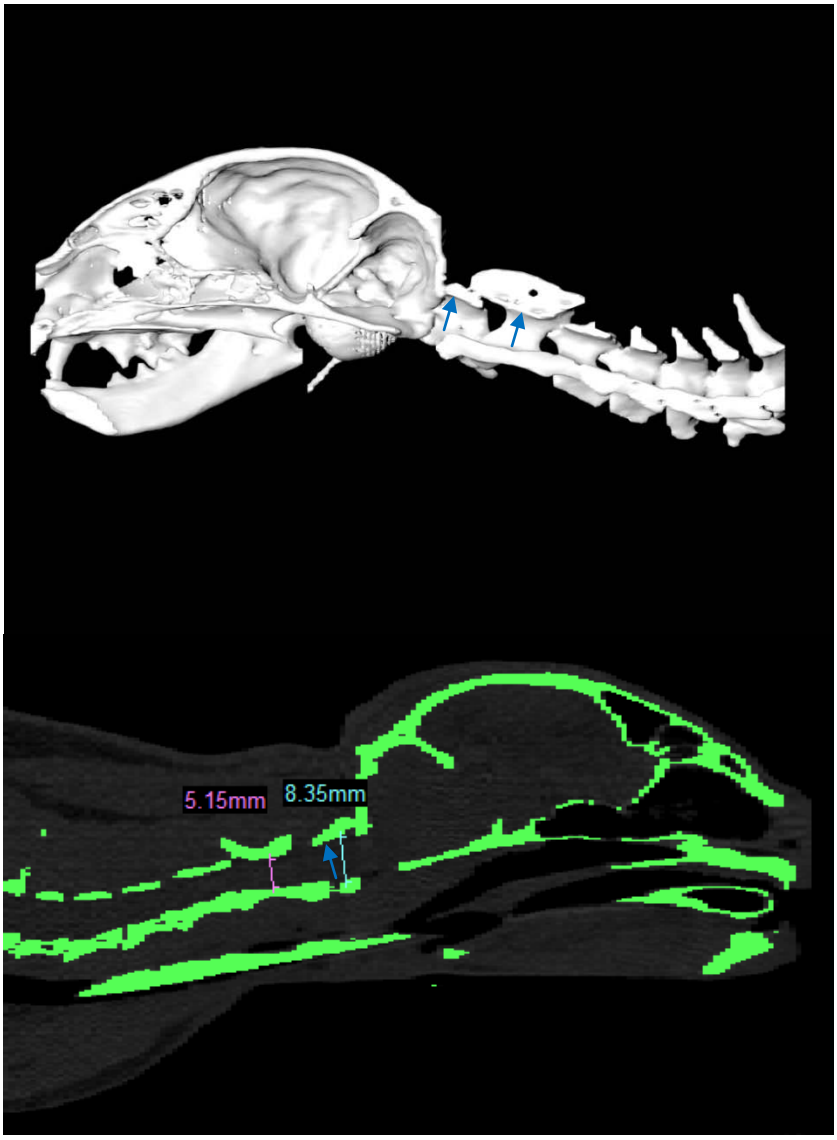

Figure 8: Representation of canal space measurement. Top: 3D reconstructed in a mid-sagittal view. Bottom: C1 and C2 canal space measurement within Mimics. Blue arrows indicate area of measurements.

Literature Review

The following review of available literature aims to demonstrate the significance of skeletal abnormalities in a wide variety of lysosomal storage diseases. GM2 is underrepresented in this literature review because few skeletal studies have been conducted in patients whose prominent clinical sign is neurologic disease. Children with GM2 demonstrate facial dysmorphism, but to date there have been few substantial studies on other skeletal abnormalities.

A retrospective study of pediatric patients with non-neuropathic Gaucher Type 1 disease found that although skeletal abnormalities varied in severity, they almost always led to "...considerable pain, disability, and poor quality of life" (Rossi *et al*, 2011). In their study, bony deformities were only second to hepatomegaly in prevalence with over 30% of patients reporting skeletal problems. Slowed growth was found in 33% of patients, and 69% of patients that underwent X-ray diagnostics had at least one detectable skeletal abnormality with complaint of pain. Nearly 8% of patients experienced osteolytic lesions. Rossi's study ultimately demonstrates that physicians of LSD patients need to monitor skeletal deformities along with other disease complications, especially if that patient is unable to voice discomfort.

A study of non-neurologic Niemann Pick disease type B consisted of 20 pediatric patients and 26 adult patients (Wasserstein *et al*, 2012). The patients underwent bone scans to measure bone mineral content and bone mineral density. Radiographs were conducted to determine relative bone age and maturity. From these bone studies researchers found 25% of pediatric patients had suffered from skeletal fractures, and 60% of pediatric patients complained of leg and back pain

from skeletal malformations. These patients also had a maturity bone delay of up to 1.6 years. Of adult patients, 53% experienced bone fractures and 58% complained of back pain associated with skeletal deformities. Results from the bone scan experiments in pediatric patients demonstrated significant differences in bone mineral content and bone mineral density in all bones scanned (hip, femoral neck, and lumbar spine) compared to healthy, unaffected children. Likewise, Niemann Pick disease type B adult patients' bone scans revealed osteopenia in nearly half of patients in all 3 bones as well as osteoporosis in 36% of adult patients' spines and 19% in adult patients' hips. It can be concluded from this study that skeletal abnormalities persist in patients with some LSDs, such as Niemann Pick disease.

Various skeletal abnormalities are found in many mucopolysaccharidoses (MPS) (types I-VII). The most common abnormalities are hypoplastic vertebral bodies leading to kyphosis, shallow acetabulae leading to sub- or full luxation of femoral heads, and broadening of clavicles and ribs (all of which are observed in GM2-cats) (White, 2011). Also, hip dysplasia is most common and unfortunately "has not been shown to respond to stem cell or enzyme replacement therapy...ultimately requiring corrective surgery." Most interesting is White's observation of spinal cord compression in nearly all cases of pediatric MPS stating that the compression is so severe that it is potentially life-threatening. Lastly, short stature is a common skeletal deformity in patients with MPS, and unfortunately treatments such as enzyme replacement therapy are unsuccessful at entirely alleviating skeletal issues. However, it is important to note that the earlier skeletal malformations are detected, the more successful treatment can become at alleviating any *progression* in skeletal malformations.

An additional study of MPS (type's I-IV, VI) reported that 43% of 30 patients studied complained of skeletal pain, 67% of joint stiffness, and 47% of kyphosis (Lin *et al*, 2013). Interestingly, 93% of patients suffered from vertebral deformities, 47% from vertebral instability, and 43% from spinal cord compression. These same patients were given a bone scan that revealed low bone mineral density in all patients as well as short stature. In contrast to previously reviewed articles, Lin *et al* reported that 8 patients underwent enzyme replacement therapy after the initial studies, and all of the 8 patients demonstrated an increase in bone mineral density. It is important to note that bone mineral density did increase with enzyme replacement therapy; although pre-existing skeletal manifestations such as vertebral deformities were not corrected, and therefore remain unresolved at present. Enzyme replacement therapy is only able to stop or substantially slow skeletal disease progression. This is backed by Lin's statement that all of the older patients in the cohort of 30 showed lower standard scores of all parameters (height, weight, and body mass index) strongly suggesting that skeletal disease progression is rapid, aggressive, and incurable with current therapies. However, some patients are good candidates for surgical procedures to control pain and/or alleviate skeletal stress.

A study of MPS VII (β-glucuronidase deficiency) was conducted using canine models. Several diagnostic tests were performed such as radiographs and gross evaluation and histochemical staining of tissues (Xing *et al*, 2013). Radiograph evaluation found that untreated animals demonstrated complete coxofemoral joint luxation, whereas MPS VII treated (hepatocyte growth factor or gamma retroviral vector therapies) and normal subjects' demonstrated significantly reduced luxation of coxofemoral joints. Additionally, osteophyte formation was not significant

in untreated animals due to their shortened life span (2 years). In contrast, treated animals demonstrated pronounced osteophyte formation mainly due to their increase in lifespan because of successful treatment. Gross examination revealed joint mice in the coxofemoral joint of one MPS VII treated dog. Xing *et al* mentioned that joint mice (loose bony fragments within a joint) would have likely been found in all untreated and treated animals that were necropsied prior to this subject; however, they did not look closely for joint mice as this skeletal abnormality was not previously appreciated. Interestingly, the treatment did assist in easing the devastating skeletal malformations in MPS VII affected dogs when treated early. This is promising for future research in areas where skeletal deformities are prevalent and debilitating to affected subjects.

Chapter 3

Bony Abnormalities in Cats with Sandhoff Disease

Results

The following results were obtained from both 3D reconstructed skeletal models and 3D printed limb bones derived from whole-body CT scans. Spinal cord compression was of concern based on clinical features; therefore, a variety of measurements were taken to quantify compression. First, ventral lengths of specific vertebral bodies (C1, C2, T1, T2, L1, and L2) were taken from all cats to quantify bony changes in GM2 animals that may lead to spinal cord compression (Table 2B, Figures 10,12,14). This was followed by measuring canal space width to determine if a narrowed canal could result in spinal cord compression (Table 2A, Figures 9,11,13). GM2 immature cats did have significantly narrower canal space in C1 when compared to sex/age-matched normal control cats ($p=0.045$) (Table 2A, Figure 9A). No other groups demonstrated statistical differences in C1/C2 canal space. It was expected that differences would be found when comparing GM2 immature cats to GM2+AAV cats based on size difference due to age alone. The fact that canal space is no larger in adult treated animals than in juvenile untreated cats may explain spinal cord compression in the AAV-treated cohort to some degree. Significant differences in C2 ventral lengths were found between all groups.

Table 2: Vertebral Column Measurements

A	**Vertebral Column Measurements (mm)**					
	Canal Space					
GM2 Immature	**C1**	**C2**	**T1**	**T2**	**L1**	**L2**
7-1010	7.61	6.62	6.01	5.3	4.87	4.15
7-1006	6.74	6.87	6.4	3.82	3.83	3.82
7-1057	6.75	5.85	6.02	5.14	4.55	3.86
Normal Immature						
11-1015	8.05	5.57	4.98	4.07	4.32	4.44
11-1030	9.92	6.14	5.4	4.99	3.61	4.11
GM2 + AAV Mature						
11-900	6.53	5.67	7.48	8.97	6.3	5.85
7-943	6.54	7.77	6.17	6.36	4.15	4.86
7-945	7.82	8.61	5.61	5.24	4.76	4.69
7-979	8.68	6.58	5.4	4.21	4.62	4.71
Normal Mature						
8-1670	7.58	7.93	6.77	5.27	4.46	5.14
100B-909	8.48	6.07	5.49	5.22	3.66	3.76
100B-914	6.55	6.98	5.37	4.68	4.02	4.02
9-1594	7.19	6.35	5.18	4.00	4.34	4.46

B	**Vertebral Column Measurements (mm)**					
	Ventral Length					
GM2 Immature	**C1**	**C2**	**T1**	**T2**	**L1**	**L2**
7-1010	4.91	11.14	6.78	5.98	10.13	11.00
7-1006	4.10	11.05	6.24	5.13	9.99	12.16
7-1057	3.98	10.78	4.64	4.20	9.79	10.90
Normal Immature						
11-1015	4.05	15.00	9.06	7.22	11.83	14.08
11-1030	6.02	16.11	8.92	9.06	13.14	14.46
GM2 + AAV Mature						
11-900	3.01	12.66	7.19	7.15	12.09	13.07
7-943	4.99	15.07	6.15	5.99	15.08	16.23
7-945	4.26	13.41	5.59	4.11	11.36	12.68
7-979	5.04	15.06	7.05	5.14	13.12	15.15
Normal Mature						
8-1670	6.01	18.26	10.00	9.06	15.53	16.80
100B-909	4.02	15.89	7.63	8.63	11.88	11.22
100B-914	5.33	18.58	9.38	8.17	13.32	14.23
9-1594	4.94	16.06	8.68	9.92	12.55	12.92

Table 2: A: Canal length. B: Ventral length. Measurements in millimeters (mm).

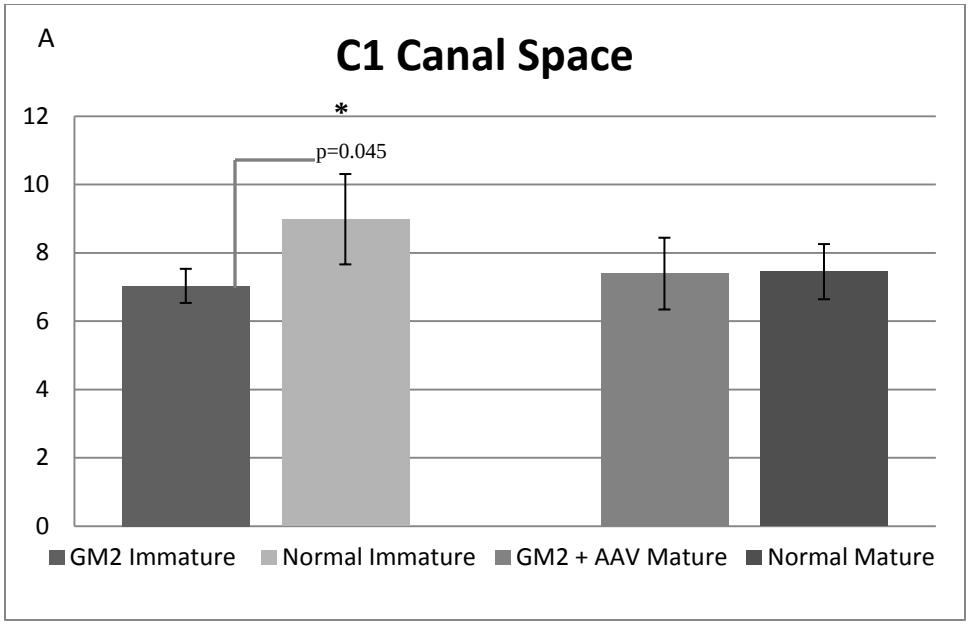

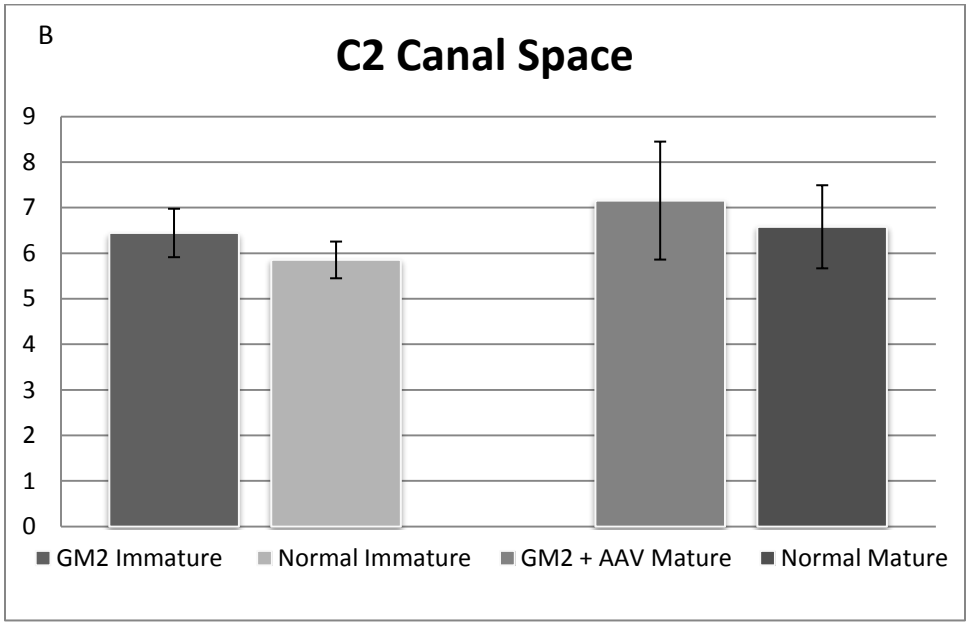

Figure 9A:C1 canal space. GM2 immature animals have a narrower canal space compared to normal (grey line), measured in mm.

Figure 9B:C2 canal space. No significance was measured between the treatment groups.

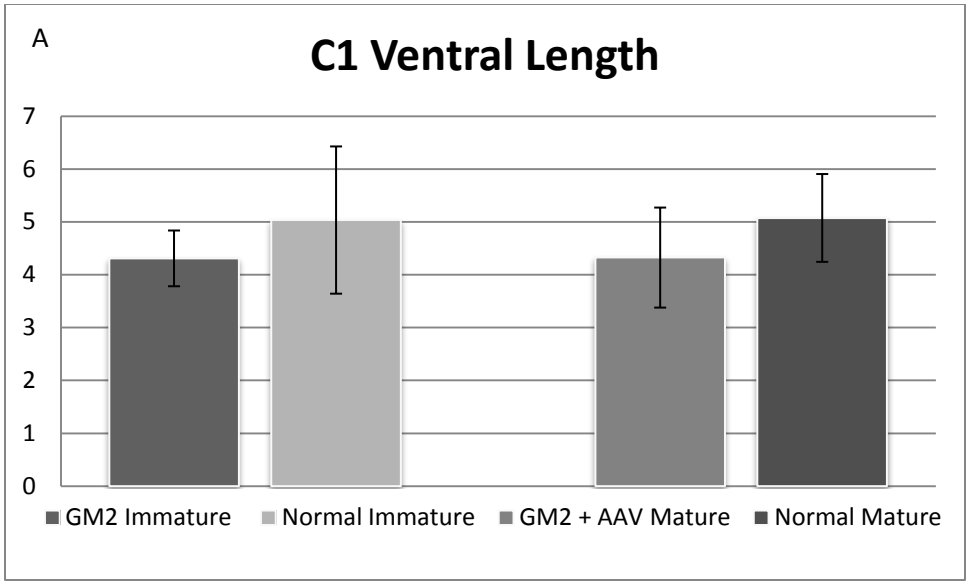

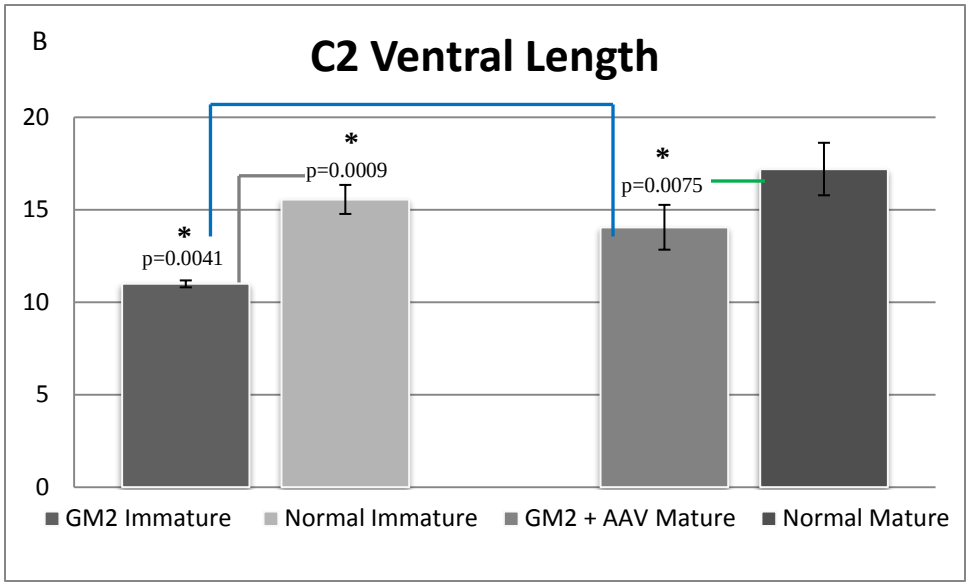

Figure 10A: C1 ventral length. Though statistical difference was not achieved, note that C1 lengths in both affected groups appear to be shorter than normal controls. This is consistent with gross CT observation, measured in mm.

Figure 10B: C2 ventral length. * depicts 1-tailed t-test comparing the following groups: GM2 immature compared to treated (blue line), or normal control (grey line) and GM2+AAV compared to sex/age-matched normal control (green line).

Upon statistical analysis of thoracic vertebrae, significance was achieved due to a widening of canal space in GM2 immature cats compared to normal controls (Figure 11A). GM2 immature cats' ventral lengths (T1: 5.9±1.11; T2: 5.1±0.89) were significantly shortened when compared to normal controls in both T1 (8.99±0.10; p=0.017) and T2 (8.14±1.30; p=0.039) (Figure 12).

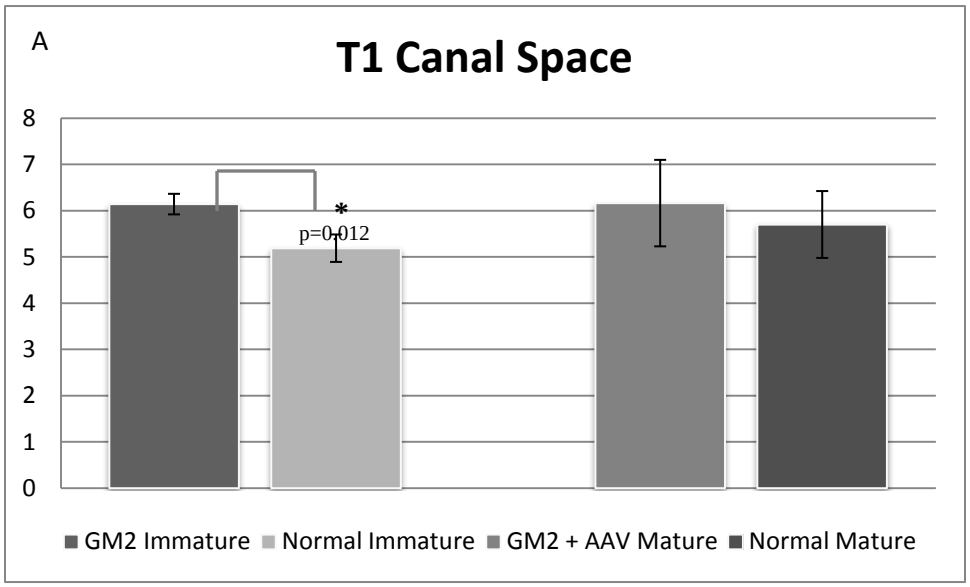

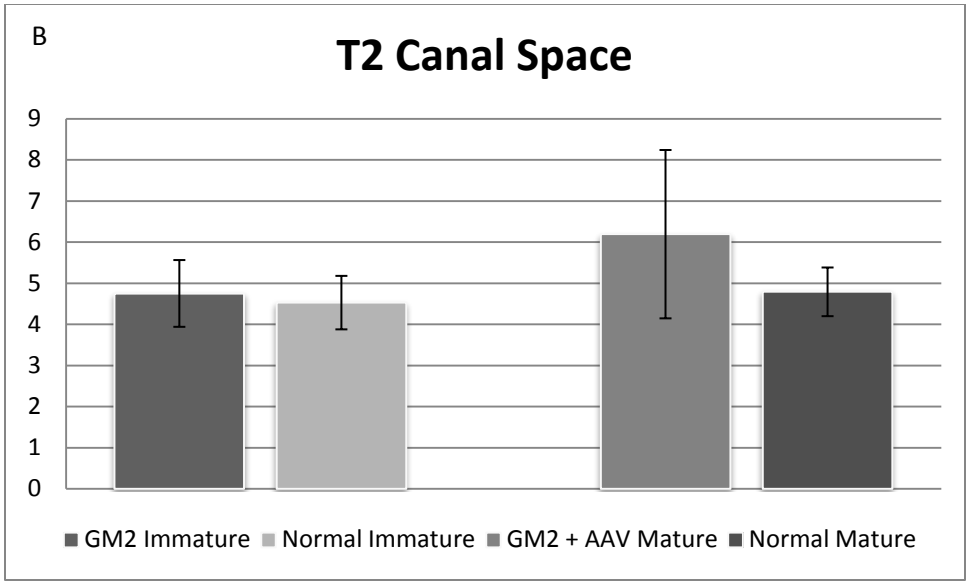

Figure 11A: T1 canal space. Significance was measured between GM2 immature cats compared to sex/age-matched normal controls (grey line), measured in mm.

Figure 11B: T2 canal space. No significance was measured among groups.

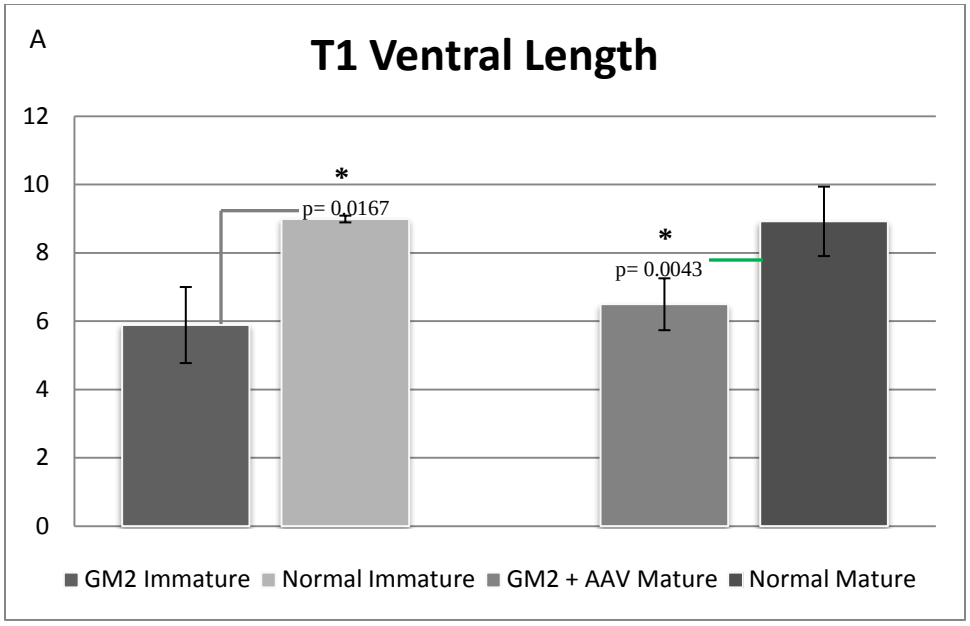

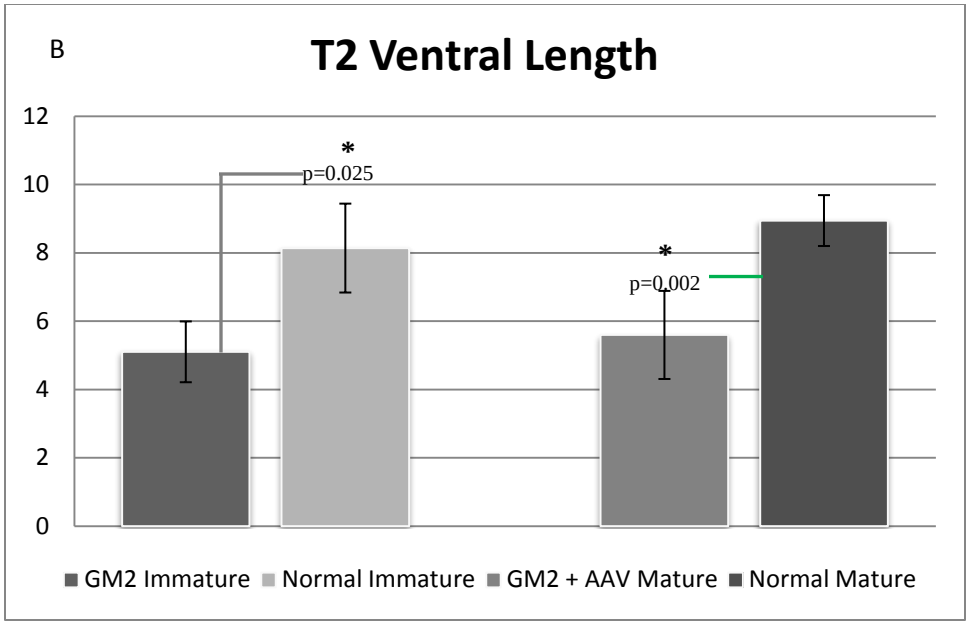

Figure 12A:T1 ventral length. Significance was measured between both GM2 immature (grey line) and GM2+AAV cats (green line) when compared to sex/age-matched normal controls, measured in mm.

Figure 12B:T2 ventral length. GM2 immature (grey line) and GM2+AAV (green line) cats' ventral vertebral length was shorter compared to normal control.

Lastly, L2 canal space was significantly different between GM2 immature and GM2+AAV cats (Figure 13B). Ventral length was significantly shortened between GM2 immature compared to GM2+AAV and normal immature cats at L1 and L2 (Figure 14). No significance was measured when comparing GM2+AAV cats to sex/age-matched controls at the lumbar measurements.

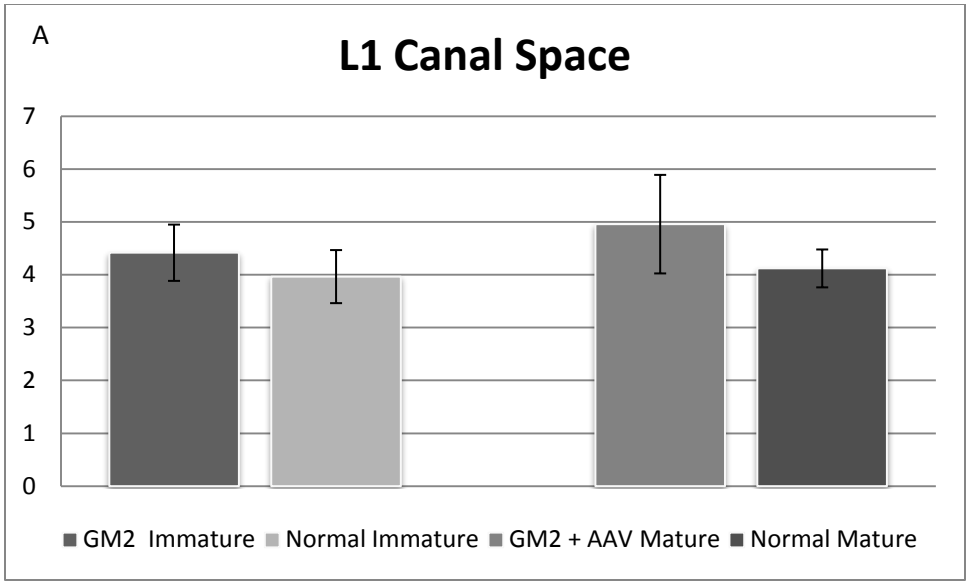

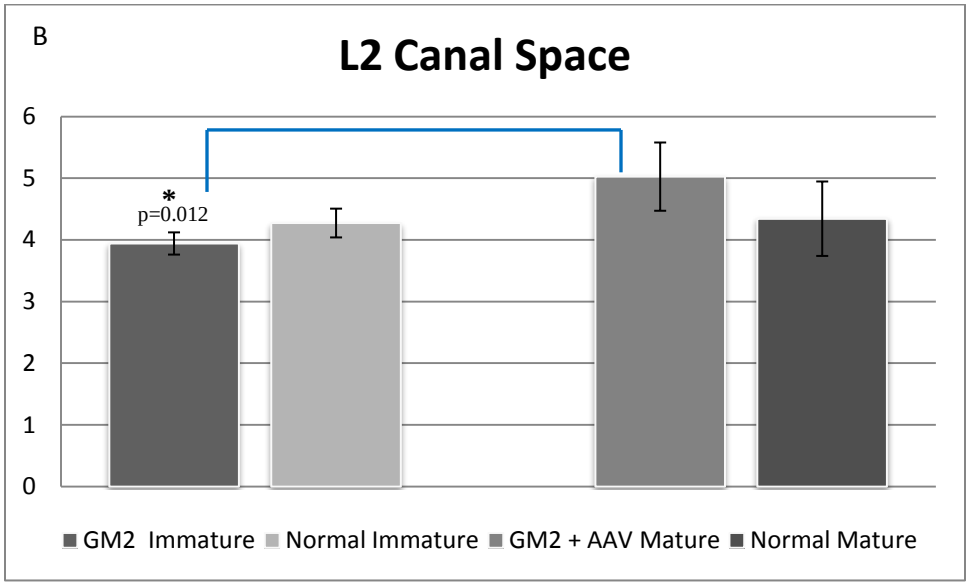

Figure 13A:L1 canal space. Significant differences were not detected between any groups, measured in mm.

Figure 13B:L2 canal space. Significance was measured comparing GM2 immature to GM2+AAV cats (blue line).

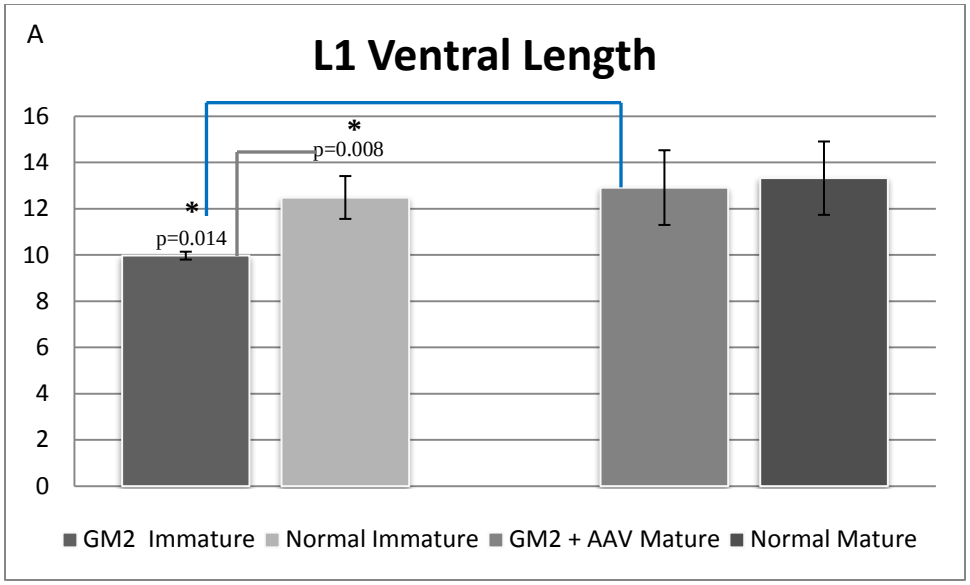

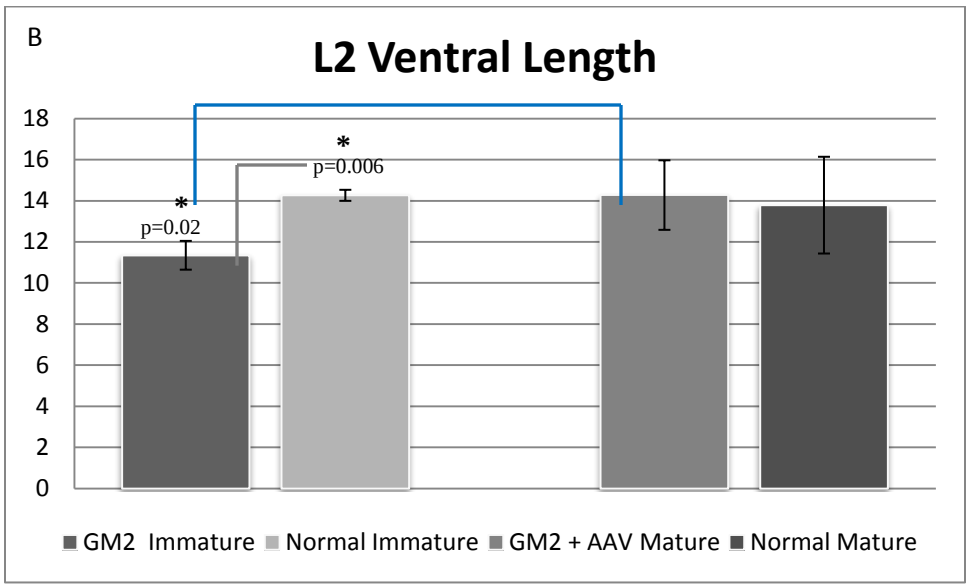

Figure 14:L1 ventral length. Immature GM2 immature cats were significantly different from both sex/age-matched controls (grey line) and GM2+AAV cats (blue line), measured in mm.

Figure 14B:L2 ventral length. GM2 immature cats were significantly different from both sex/age-matched controls (grey line) and GM2+AAV cats (blue line), measured in mm.

In addition, C1/C2, T1/T2, and L1/L2 spinal cord segments were measured for signs of spinal cord compression that may lead to the overt limb weakness demonstrated in the older GM2+AAV cats (Table 3; Figure 15). When comparing GM2 immature cats to GM2+AAV cats, untreated cats' spinal cords were narrower in the lumbar region probably due to age difference. However, GM2 immature animals were not significantly different than mature GM2+AAV treated cats in the cervical and thoracic areas which may be a component of an overall skeletal stunting of GM2 cats compared to normal controls. Although GM2 immature cats did not demonstrate any significant spinal cord compression at any site compared to normal sex/age-matched controls, GM2+AAV cats did exhibit a narrower cervical spinal cord compared to sex/age-matched normal controls ($p=0.022$). Thoracic and lumbar sites of GM2+AAV cats trended narrower than normal, but were not significantly different. These findings are consistent with previous MRI diagnostics in that cervical spinal cord between C1-C3 is compressed in some GM2+AAV cats to the degree of interrupting cerebrospinal fluid (CSF) flow.

Table 3: Spinal cord compression site

	Spinal Cord Measurements (mm)		
	Compression Site		
GM2 Immature	**C1/C2**	**T1/T2**	**L1/L2**
7-1010	7.43	5.96	4.41
7-1006	6.30	5.61	3.17
7-1057	8.67	6.21	5.14
Normal Immature			
11-1015	6.28	6.74	4.40
11-1030	7.73	6.27	5.10
GM2 + AAV Mature			
11-900	6.71	5.88	6.10
7-943	6.26	5.64	6.17
7-945	6.79	5.72	5.78
7-979	7.42	4.96	4.58
Normal Mature			
8-1670	9.38	9.22	5.68
100B-909	7.55	6.27	5.90
100B-914	7.88	8.50	6.21
9-1594	8.70	5.11	5.77

Table 3: Measurements are taken from a lateral view from dorsal to ventral aspect of spinal cord, avoiding discs or dorsal root ganglia (DRG) when necessary. Measurements in mm.

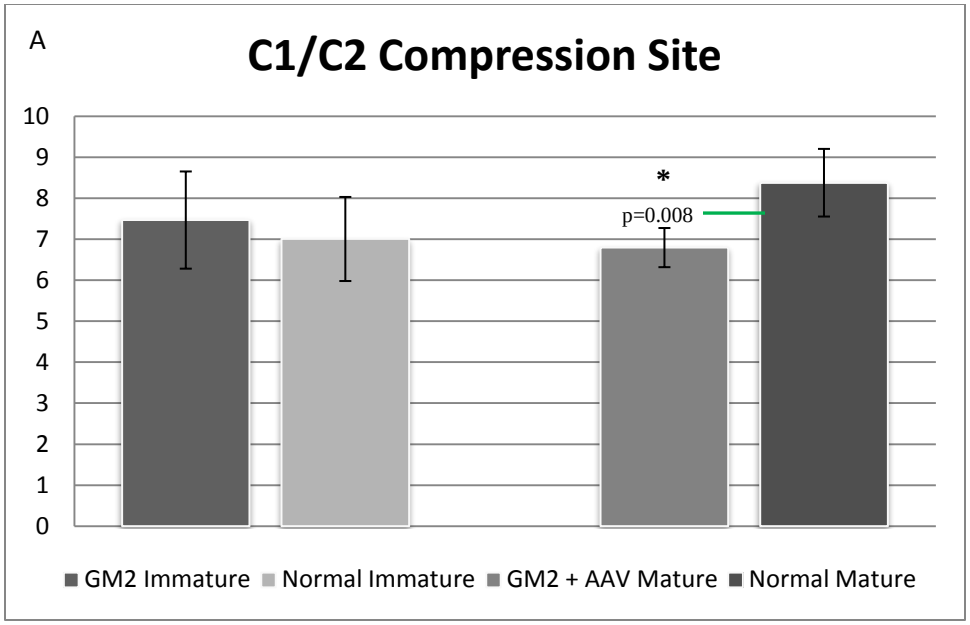
A
C1/C2 Compression Site
10
9
8
7
6
5
4
3
2
1
0
*
p=0.008
GM2 Immature
Normal Immature
GM2 + AAV Mature
Normal Mature

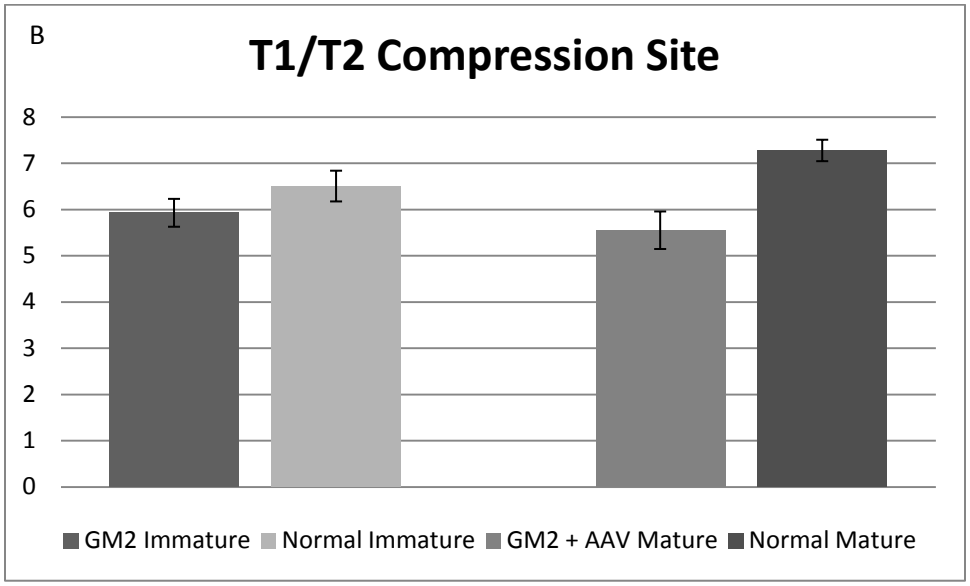
B
T1/T2 Compression Site
8
7
6
5
4
3
2
1
0
GM2 Immature
Normal Immature
GM2 + AAV Mature
Normal Mature

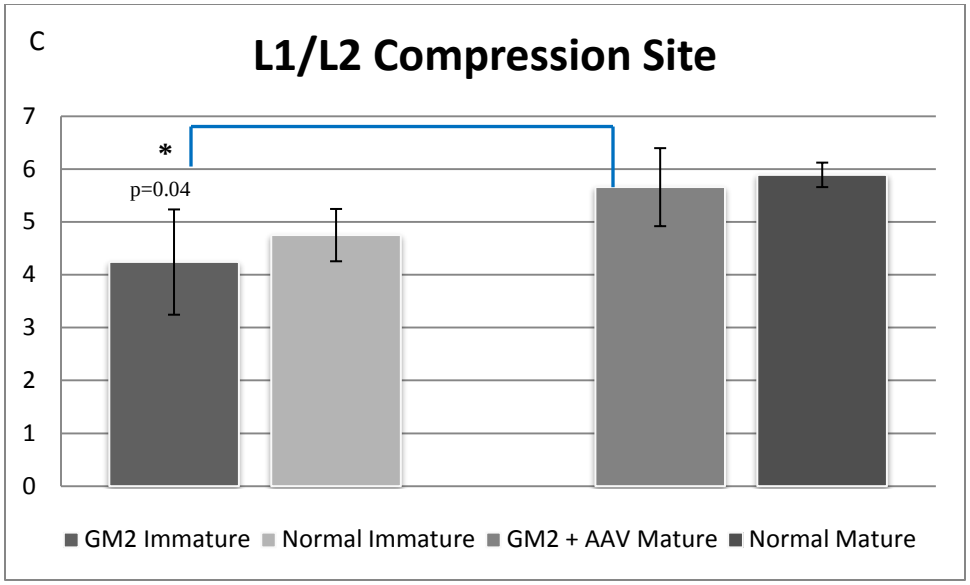

Figure 15A:C1/C2 compression site. Significance was measured between GM2+AAV cats compared to sex/age-matched normal controls (green line). This is consistent with necropsy findings as C1-C3 spinal cord segments are compressed consistently in most GM2+AAV cats, measured in mm from dorsal to ventral aspect of segment.

Figure 15B:T1/T2 compression site. GM2 immature animals are not significantly different in spinal cord compression sites compared to sex/age-matched normal controls. GM2+AAV cats' thoracic compression site is trending toward significance compared to normal mature cats with a p-value of 0.06.

Figure 15C:L1/L2 compression site. No difference in spinal cord compression sites between GM2 affected animals and normal controls. Significance was measured between GM2 immature and GM2+AAV cats. Note that L1/L2 site is normalized in GM2+AAV animals, which is consistent with vertebral measurements.

Although spinal cord compression is concerning, long bone abnormalities are also of concern because they may result in limb weaknesses, leading to premature humane endpoint in GM2+AAVcats. Both left and right femurs were measured to compare GM2 cats to their normal controls (Table 4; Figure 16). As expected GM2 immature cats' femoral lengths were significantly different from GM2+AAV cats' probably due to vast age differences rather than

disease. Statistics of GM2 immature femoral lengths compared to sex/age-matched normal controls revealed that affected cats' femurs were significantly shorter (Left p=0.016, Right p=0.014). This was consistent with overall gross observation of limbs as well. There was no statistical difference between GM2+AAV cats and sex/age-matched controls. This also was consistent with grossly observed findings in that femoral lengths tended to be about the same in both treated and normal cats; however, proximal and distal ends of the femoral shaft of treated animals appear to be narrower than normal. Shaft narrowing is not observed in untreated cats compared to normal (Figures 4&5).

Table 4: Femur measurements

	Long Bone Measurements (mm)	
	Femur	
GM2 Immature	**Left**	**Right**
7-1010	84.0	84.0
7-1006	71.5	71.5
7-1057	74.0	74.0
Normal Immature		
11-1015	94.0	95.0
11-1030	100.0	100.0
GM2 + AAV Mature		
11-900	101.0	101.0
7-943	108.0	109.0
7-945	103.0	103.0
7-979	105.0	105.0
Normal Mature		
8-1670	120.0	120.0
100B-909	103.0	103.0
100B-914	115.0	111.0
9-1594	104.5	104.5

Table 4: Length measured with calipers using absolute bone length. Measured in mm. Note GM2+AAV cats' femoral lengths are normalized comparing to normal controls.

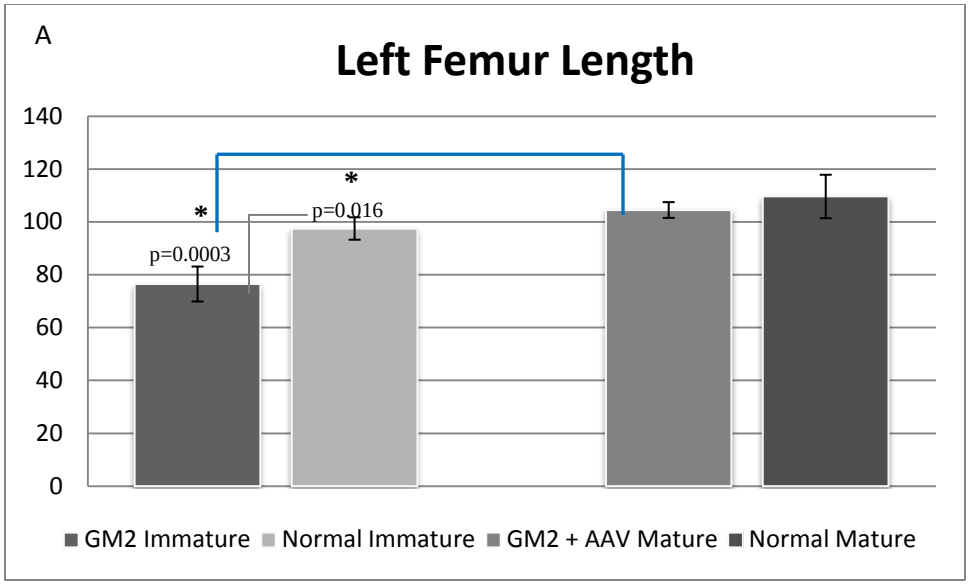

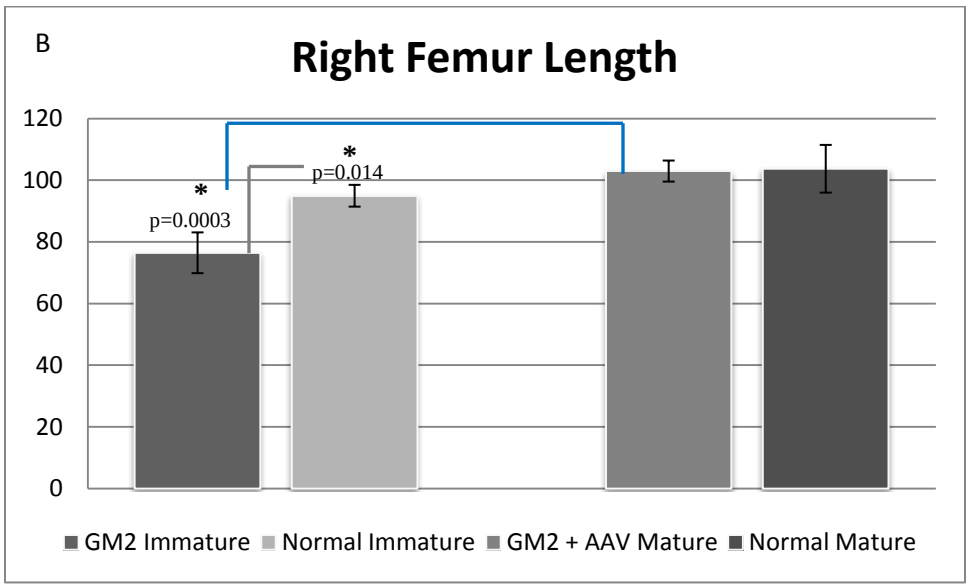

Figure 16A: Average left femoral length. Significance was measured between immature GM2 immature and GM2+AAV cats (blue line) and between GM2 immature and immature normal cats (grey line).

Figure 16B: Average right femoral length. Results are similar to 16A.

Additionally, lengths of tibia were measured, and results were consistent with femoral length findings (Table 5; Figure 17). Tibial lengths were shorter in GM2 immature (80.33±4.16 mm) versus GM2+AAV cats (103±8.52 mm). Again, vast age difference probably plays a large factor in this measurement, as the untreated cats are ~4.5 months of age and are still growing. Both left and right tibial lengths were shorter in GM2 immature cats compared to sex/age-matched normal controls (left and right p=0.006). GM2+AAV tibial lengths are also significantly shorter as compared to normal (left and right p=0.02).

Table 5: Tibia measurements

	Long Bone Measurements (mm)	
	Tibia	
GM2 Immature	**Left**	**Right**
7-1010	85.0	85.0
7-1006	79.0	79.0
7-1057	77.0	77.0
Normal Immature		
11-1015	99.0	99.0
11-1030	106.0	107.0
GM2 + AAV Mature		
11-900	106.0	106.0
7-943	111.0	111.0
7-945	104.0	105.0
7-979	91.0	91.0
Normal Mature		
8-1670	121.0	119.0
100B-909	114.0	115.0
100B-914	119.5	119.5
9-1594	109.0	109.0

Table 5: Absolute bone length measured with calipers. Measured in mm. Note shortened lengths of GM2 cats compared to normal controls.

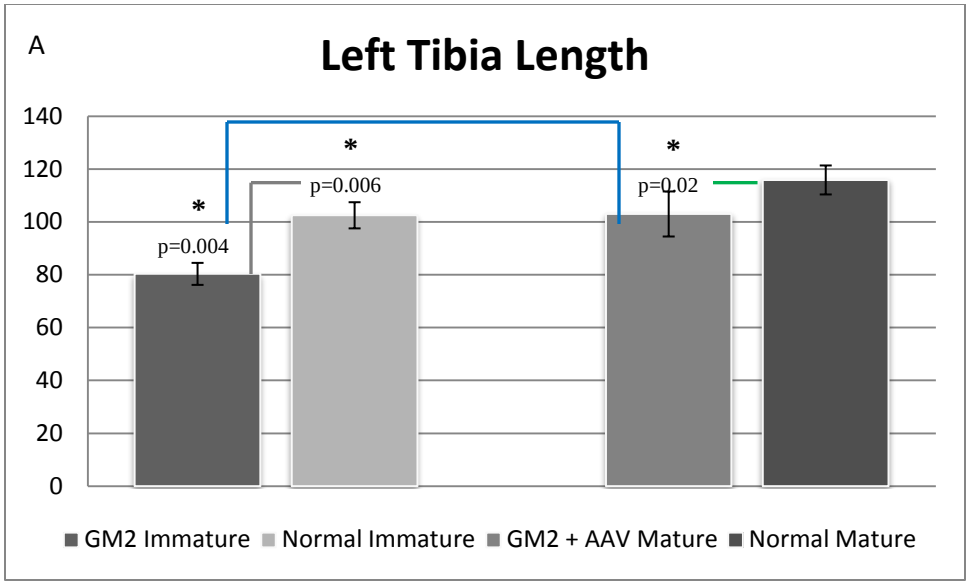

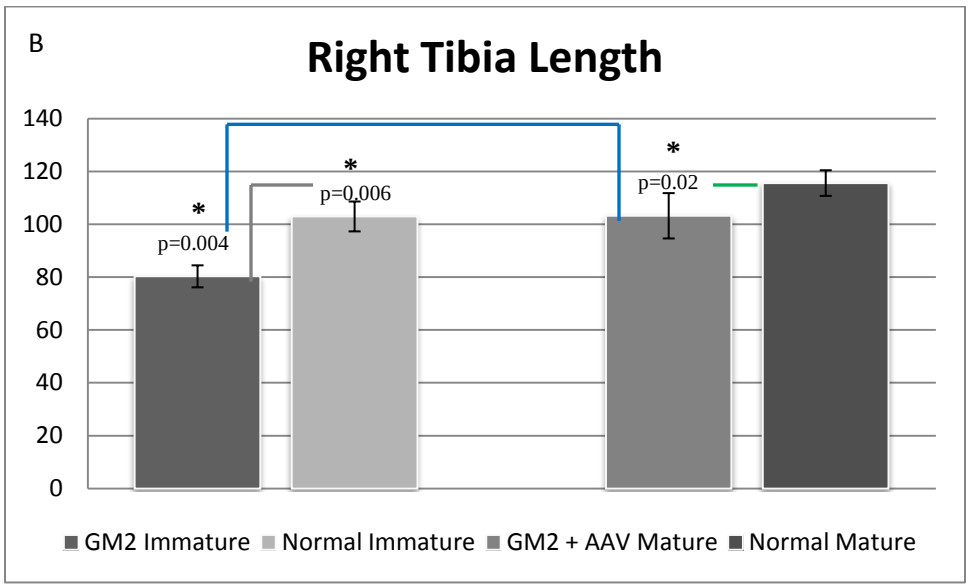

Figure 17A: Average left tibial length. Significance was measured between GM2 immature and GM2+AAV cats (blue bar), as well as GM2 immature and treated as compared to respective sex/age-matched normal controls (grey and green bars), measured in mm.

Figure 17B: Average right tibial length. Significance was measured between GM2 immature, treated (blue bar), and respective normal controls (grey and green bars).

Thoracic limb bones were measured similarly, yet statistics revealed slightly different changes than seen in pelvic limb bones. Humeral measurements were significantly different between GM2 immature and GM2+AAV cats, and between GM2 cats and normal controls (Table 6, Figure 18).

Table 6: Humerus measurements

	Long Bone Measurements (mm)	
	Humerus	
GM2 Immature	**Left**	**Right**
7-1010	75.0	75.0
7-1006	65.0	66.0
7-1057	66.0	66.0
Normal Immature		
11-1015	86.0	86.5
11-1030	90.0	91.0
GM2 + AAV Mature		
11-900	84.5	84.5
7-943	90.0	90.0
7-945	88.0	87.0
7-979	91.0	92.0
Normal Mature		
8-1670	103.0	103.0
100B-909	100.5	100.5
100B-914	105.0	106.0
9-1594	95.0	95.0

Table 6: Absolute bone length measured with calipers. Measured in mm. Note shortened lengths of GM2 cats compared to normal controls.

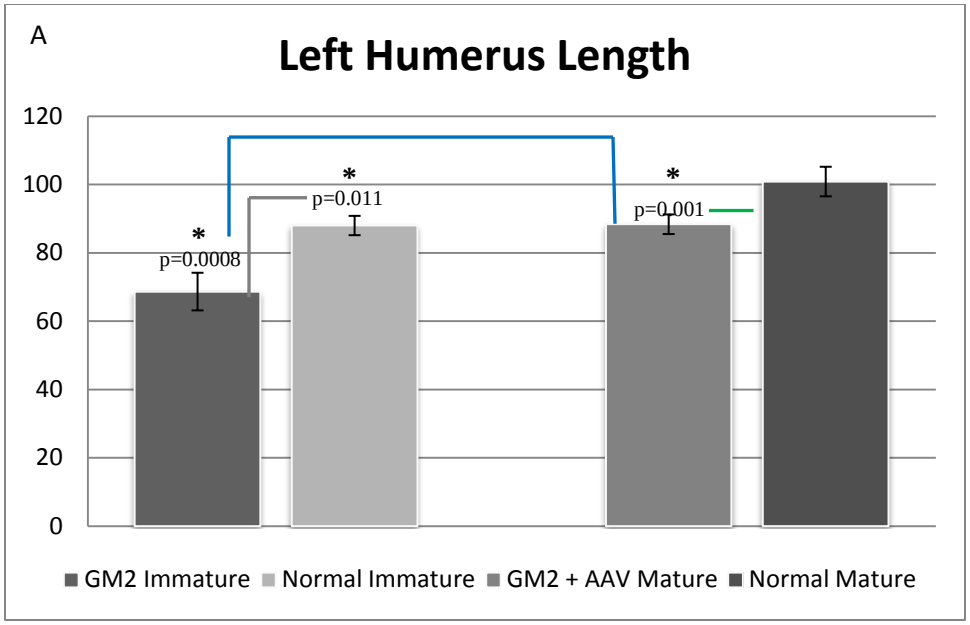

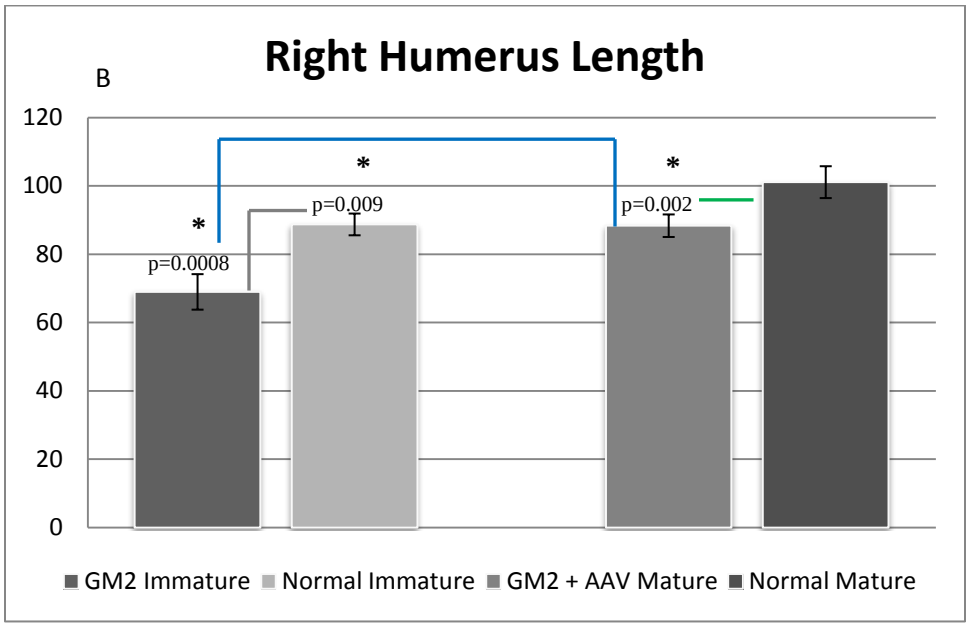

Figure 18A: Average left humeral lengths. Significance was measured between GM2 immature and GM2+AAV (blue bars) and between GM2 immature and GM2+AAV cats as compared to normal controls (grey and green bars), measured in mm.

Figure 18B: Average right humeral lengths. Similar results were obtained to those for the left humerus.

Similar results were obtained for both ulna and radius (Tables 7&8; Figure 19) where significance was measured between GM2 immature (ulna: 73.3±8.08; radius: 62.0±5.29) and treated (ulna: 100.13±3.22; radius: 84.5±1.91) animals and between GM2 immature animals and sex/age-matched normal controls (left ulna: p=0.014; left radius: p=0.013). Additionally, GM2+AAV ulnar lengths were significantly different than normal controls (left and right p=0.001).

Table 7: Ulna measurements

	Long Bone Measurements (mm)	
	Ulna	
GM2 Immature	**Left**	**Right**
7-1010	82.0	83.0
7-1006	72.0	73.5
7-1057	66.0	66.0
Normal Immature		
11-1015	96.5	94.5
11-1030	100.0	99.5
GM2 + AAV Mature		
11-900	97.0	96.5
7-943	104.0	102.0
7-945	98.0	98.0
7-979	101.5	103.5
Normal Mature		
8-1670	119.0	121.0
100B-909	114.0	113.5
100B-914	111.5	111.5
9-1594	109.0	110.0

Table 7: Absolute bone length measured with calipers. Measured in mm. Note shortened lengths of GM2 cats compared to normal controls.

Table 8: Radius measurements

	Long Bone Measurements (mm)	
	Radius	
GM2 Immature	**Left**	**Right**
7-1010	68.0	68.0
7-1006	60.0	60.5
7-1057	58.0	58.0
Normal Immature		
11-1015	77.5	75.5
11-1030	82.0	82.0
GM2 + AAV Mature		
11-900	84.0	82.0
7-943	86.0	86.0
7-945	82.0	83.0
7-979	86.0	87.0
Normal Mature		
8-1670	101.0	100.0
100B-909	99.0	99.0
100B-914	96.0	96.0
9-1594	91.0	90.5

Table 8: Absolute length measured with calipers. Measured in mm. Note shortened lengths of GM2 cats compared to normal controls.

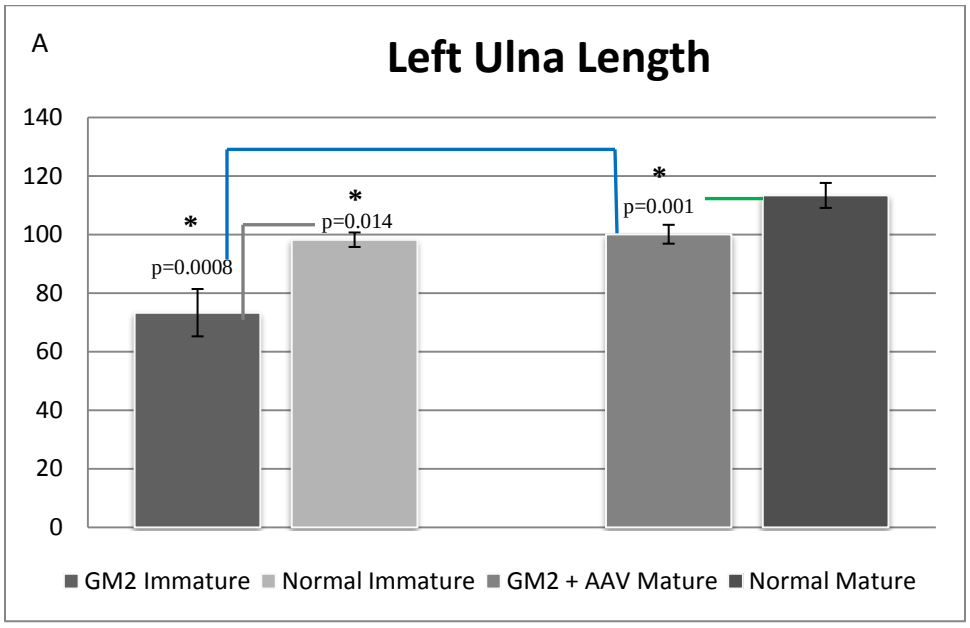
A
Left Ulna Length
140
120
100
80
60
40
20
0
*
p=0.0008
*
p=0.014
*
p=0.001
GM2 Immature
Normal Immature
GM2 + AAV Mature
Normal Mature

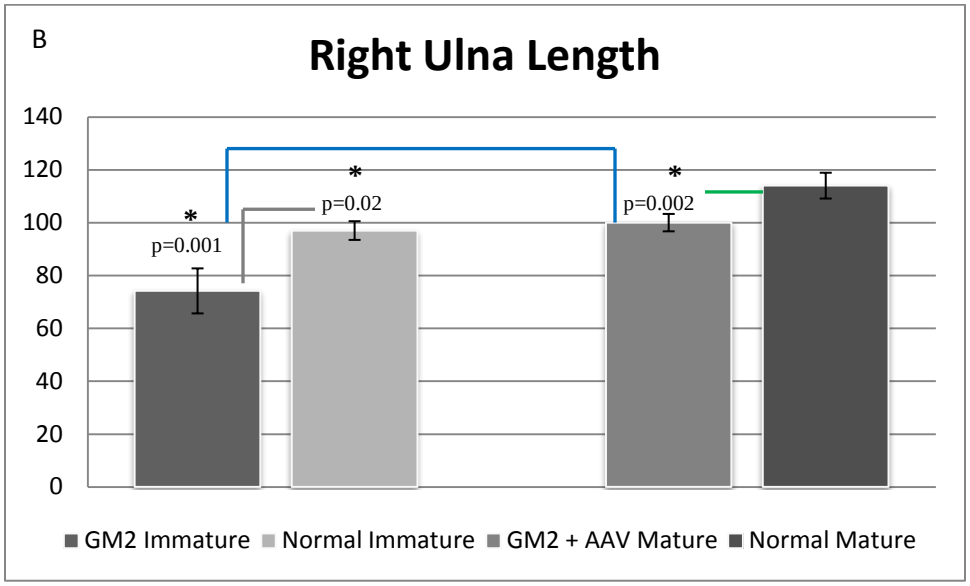
B
Right Ulna Length
140
120
100
80
60
40
20
0
*
p=0.001
*
p=0.02
*
p=0.002
GM2 Immature
Normal Immature
GM2 + AAV Mature
Normal Mature

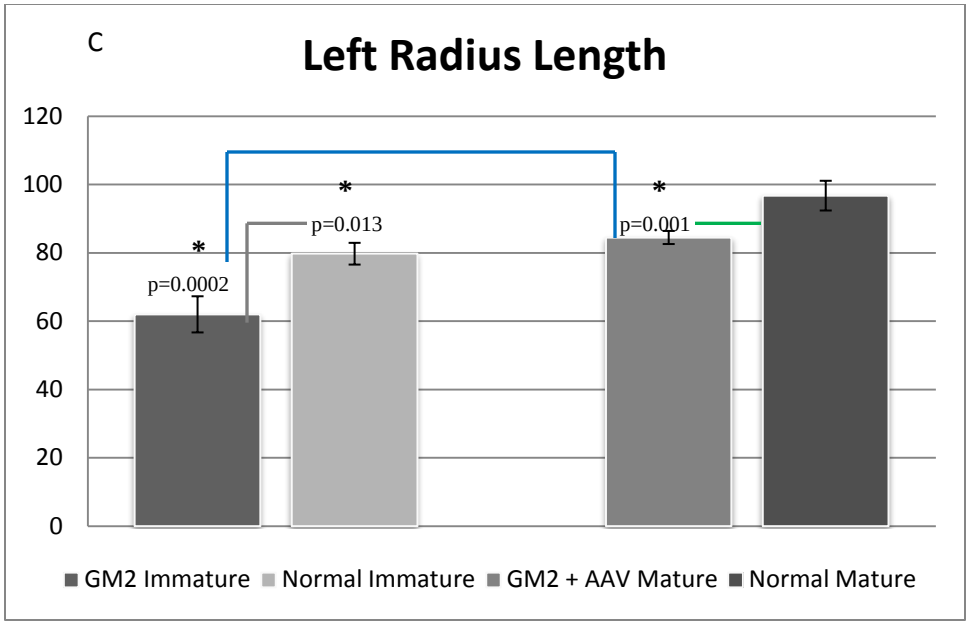

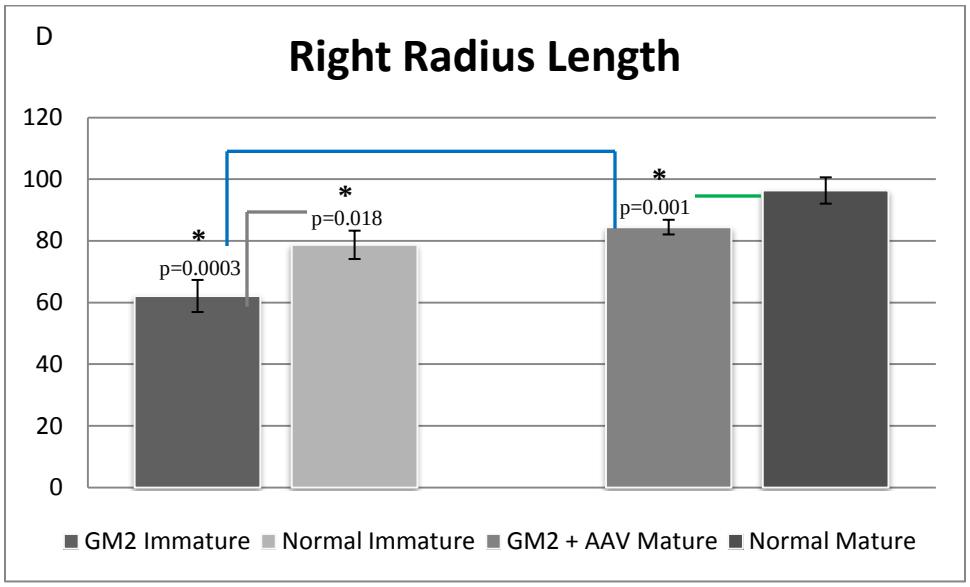

Figure 19A and B: Average left and right ulnar lengths. Significance was measured between GM2 immature, GM2+AAV cats (blue bar), and respective sex/age-matched normal controls (grey and green bars), measured in mm.

Figure 19C and D: Average left and right radial lengths. Results are similar to those obtained for the ulna.

Discussion

The goal of this project was to quantify bony changes between GM2 cats compared to normal controls. Before CT scans were performed and measurement studies were conducted, only subjective changes had been noted using radiographs, gait analyses, and MRI. Unfortunately, these diagnostics were not able to quantify changes statistically due to a lack of objective sensitive measuring equipment. Mimics imaging software and the 3D printed images have made measuring bony changes much more precise and more reliable than previous software. Prior studies conducted with pelvic radiographs of GM2+AAV cats revealed subluxated coxofemoral joints due to a shallow acetabulum, bilateral tibial bowing, and patellar luxation resulting in medially deviated hocks. Spinal radiographs revealed stunting of vertebral spinous and transverse processes, and bony bridging of cervical vertebrae. However, the majority of skeletal abnormalities were unappreciated until full body CT scans were conducted (Figure 20).

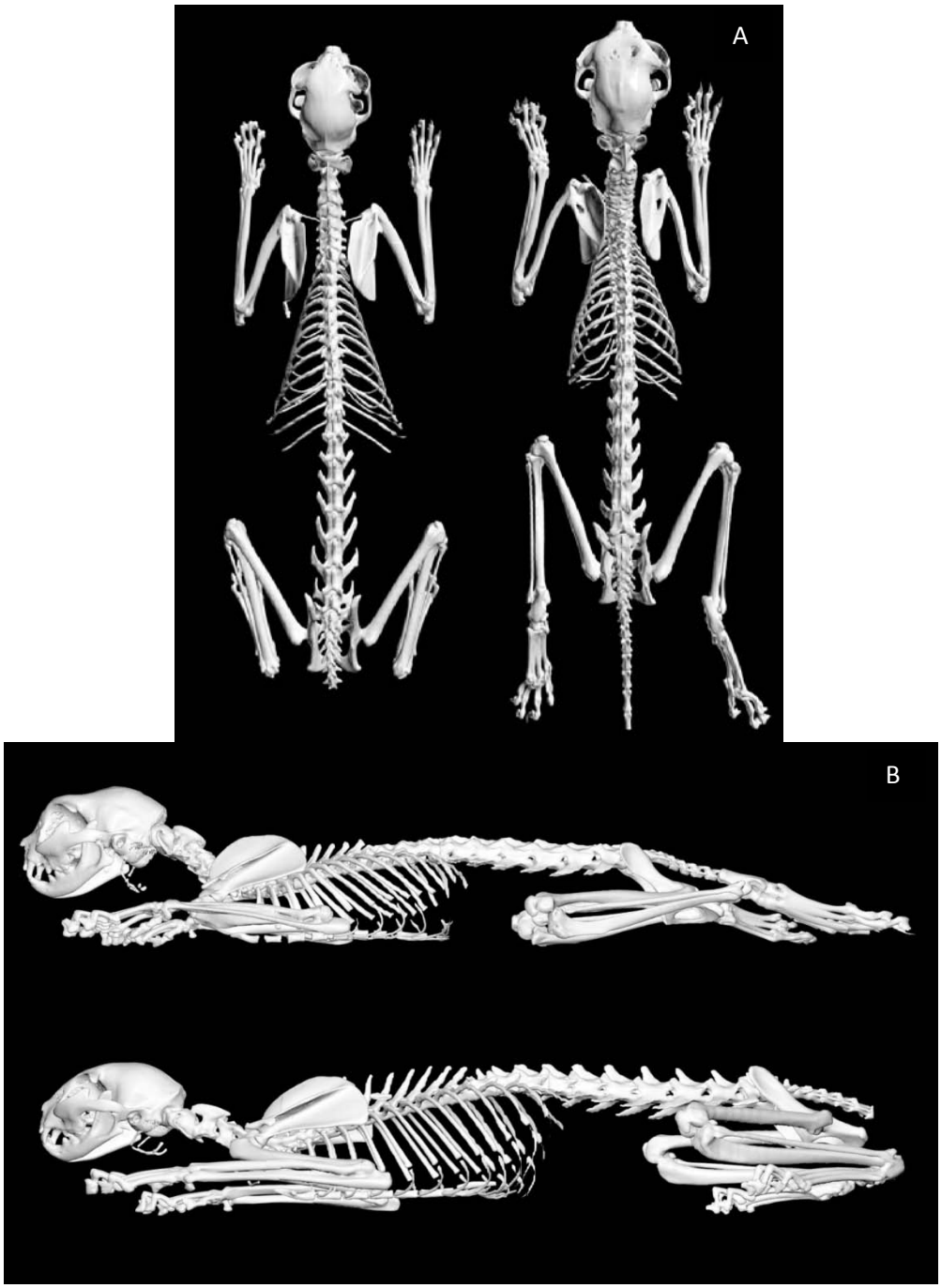

Figure 20: 3D reconstructed full skeleton. A: Dorsal view of whole skeleton. Left: Normal control female at 17 months; right: GM2+AAV female at 17 months. B: Left lateral view. Top: GM2+AAV female; bottom: normal control female. Note differences in nearly all SD bones compared to normal. *See figure 2&3 for detailed information.*

Although this study did not demonstrate a tibial bow in GM2+AAV cats compared to sex/age-matched controls, limb length was significantly different in all GM2 cats compared to normal controls. GM2+AAV cats in this study did not demonstrate tibial bowing yet had narrowing of proximal and distal long bone shafts. Though a therapeutic effect of AAV-gene therapy on tibial bowing was not conclusive in the current study, GM2+AAV cats had patellar luxation with medially deviated hock joints, which is often a precursor to tibial bowing. Therefore, we hypothesize that AAV-gene therapy substantially delayed the onset of tibial bowing.

The vertebral column and spinal cord were examined because it was previously hypothesized that spinal cord compression in GM2 cats is secondary to bony over proliferation of vertebrae, especially cervical, since T2 weighted MRI studies showed dorsal to ventral spinal cord compression. However, this study found no evidence that abnormal vertebrae cause spinal cord compression. Nevertheless, measurements of the spinal cord itself revealed compression that was significant in the cervical region and trended toward significance in the thoracic region of GM2+AAVcats as compared to normal age/sex-matched controls.

Pelvic limb long bones were measured because an overt pelvic limb weakness is one of the first clinical signs in GM2+AAV cats. Quantifying the results suggests a possible explanation of an overall smaller stature in GM2 cats and that weaknesses may be caused by the abnormal morphology of the bone shaft, causing abnormal weight bearing forces. Although thoracic limb weaknesses occur less frequently in GM2+AAVcats, clinical presentation is more severe than pelvic limb weakness in that range of motion (ROM) in the elbow joint is decreased, leading to

contracture and difficulty ambulating. Thoracic limb measurements were consistent with pelvic limb measurements. Abnormal weight forces and abnormal muscle attachments may be the cause of such clinical signs. A GM2+AAV cat (7-945, Table 1) developed bilateral elbow contracture, causing difficulty in ambulation. ROM was very limited in both elbow joints. Necropsy findings revealed the brachialis muscle had abnormal insertions on the radius and ulna (normal insertions being radial tuberosity and ulnar tuberosity, respectively) (Evans, 1993). It is hypothesized that this abnormal muscle attachment led to some of this animal's thoracic limb abnormalities. Necropsy findings from several GM2+AAV cats revealed an abnormal radial process distal to the radial tuberosity. The abnormal muscle attachment is thought to be causing abnormal tension on the radius, resulting in inappropriate bone growth. This can be explained using Wolfe's Law as defined by Blood and Studdert: skeletal transformation is dependent upon the exertion of pressures (Blood *et al*, 1999). If pressure and tension are placed correctly on the respective bone, then each bone works together to make a sound, efficiently functioning frame in which the animal is able to support body weight, ambulate, and carry out everyday tasks. However, abnormal pressures and tensions on bone result in an inefficient frame causing potentially debilitating effects on the skeleton ultimately resulting in an animal's inability to support body weight and eventually prohibiting it from ambulating. Additionally, the previously mentioned cat's littermate, 7-943 (Table 1), demonstrated marked hind limb weakness with little thoracic limb weakness. Aberrant muscle insertion was not observed at necropsy.

It is interesting that significant differences were not *always* seen between GM2-immature and treated cats even though there were vast age differences (4-30 months) between the cohorts. It

can be hypothesized that because treated animals are living longer due to successful CNS treatment, sub-therapeutic peripheral disease is presented, especially bone abnormalities. It is promising that progress is being made to determine the cause so that appropriate treatment can be planned.

Application in Veterinary and Human Medicine

GM2 gangliosidosis is a rare disease. However, for those affected, human and animal, it is devastating. Therefore, the search to find a treatment or cure for this disease is imperative. AAV-gene therapy is successful in treating the most debilitating aspect of the disease which is CNS involvement. The musculoskeletal abnormalities associated with GM2+AAVcats are just as devastating as the neurologic disease in GM2 immature animals, though their onset is later. Although studies are lacking in humans affected with GM2, addressing these issues in animal models may lead human research teams to explore differences in affected and non-affected human skeletons. From previous studies, it is known that a wide variety of lysosomal storage diseases result in skeletal abnormalities, which in all cases resulted in pain to the affected person. Although the feline model shows no signs of pain from skeletal abnormalities (monitored by a board-certified veterinary orthopedic surgeon), it is essential to find a way to alleviate this aspect of the disease not only to provide the animal model with an increased quality of life, but also to allow that animal to live longer so that CNS disease progression can be studied further and compared to humans. The ultimate goal of this research is to develop a human therapy that substantially increases length and quality of life.

Chapter 4

Summary

Summary

GM2 gangliosidosis is a fatal, lysosomal storage disease affecting all age ranges in humans. Currently there is no cure in humans, with only supportive care given to affected persons. Studies of GM2 have been conducted for decades to end this debilitating disease, with recent substantial progress, demonstrated in animal models of GM2 such as cats affected with Sandhoff disease. This large animal model most closely resembles the infantile form of GM2 which is the most severe, and therefore, perhaps the most challenging in which to find a treatment.

AAV-gene therapy has proven successful in treating the CNS component of SD in GM2 cats, which in turn allows them to live up to 4 times longer than GM2 immature animals which typically reach humane endpoint at 4.5 months of age. This increase in lifespan has allowed peripheral disease manifestations, such as skeletal deformities. Although skeletal abnormalities are observed in GM2 immature cats, they are much less severe than in long-living GM2+AAV cats. Differences quantified in GM2 immature and GM2+AAV cats compared to controls, has allowed researchers to further investigate peripheral disease and develop a treatment to target it. Unfortunately, there has been little success in treatment of cervical vertebral abnormalities in GM2 cats. The mechanism behind these changes is still unknown but further research is planned. Based on previous studies, it can be concluded that although treatment is unable to

reverse any skeletal deformity, it can substantially slow or even stop skeletal disease progression in some animal models and humans. GM2+AAV femoral lengths are not different from normal controls whereas in GM2 immature animals femoral lengths are different from normal. Although differences still occur between treated and normal cats, some of the skeletal involvement appears normalized due to treatment. However, more work needs to be done to determine how much AAV-gene therapy is contributing to skeletal abnormality correction, especially since various vertebral parameters were not significantly different between GM2 immature and GM2+AAV animals. The results from this study will hopefully impact research on GM2 and other lysosomal storage diseases in order to better treat skeletal complications.

Conclusions

Prior to beginning this study, researchers expected to see changes in bones such as cervical vertebrae, pelvic limb bones, and skull. However, it became apparent from the first CT scan that all bones were affected in GM2 cats, including sesamoid bones. It can be concluded from the bony abnormality study that skeletal problems persist in both GM2 immature and GM2+AAV animals, with treated animals demonstrating a more severe skeletal involvement due to increased lifespan. Future studies will explore ways to treat bony involvement more effectively, while maintaining successful therapy of the CNS.

Limitations

To increase the n-value of mature normal controls, a carrier of GM1 gangliosidosis was used. Skeletal abnormalities are not recognized in GM1 carriers, or for that matter in affected cats with GM1 gangliosidosis. Nevertheless, it would have been preferable to have homozygous normal sex/age-matched controls as well as a larger n-value of untreated animals. Even with limited numbers of animals, statistically significant differences were documented between GM2 and normal cats. Additionally, as in all research projects, funding was a limiting factor. The cost of CT scans is high, as are the resources needed for sedation and care for the animal while undergoing a CT scan. With additional funding, sequential CT scans could have been conducted throughout the life of the animal (rather than a single scan at humane endpoint) to chart development of bony changes. For example, one subject underwent CT scanning 6 months before reaching humane endpoint, and it was noted at necropsy that this subject had osteolytic lesions on the skull not seen on CT. If a CT could have been performed on this cat prior to humane endpoint, other bony changes may have been detected.

Future Research Plans

This study is only the first step of quantifying skeletal changes in cats affected with Sandhoff disease. There are a number of aspects that still need to be explored such as rib cage conformation. Further studies need to be conducted to determine true cause of spinal cord compression. Also, CT and MRI need to be conducted sequentially so that subjects have more than one data point throughout life, allowing researchers to determine when bony changes

develop in both GM2 immature and treated cats. Lastly, histopathology should be conducted on different bone types *i.e.,* long bones, short bones, irregular bones, etc, to determine differences in bone metabolism of affected and normal subjects.

Additionally, skeletal studies should be conducted in humans affected with GM2 gangliosidosis. Since the literature is lacking in reports of this nature, it is likely that an underlying skeletal component is being overlooked due to the severity of CNS disease. However, it would be informative to compare human skeletal changes to the feline abnormalities described herein, providing a better estimate of how accurately the feline model represents the human condition. A wide spectrum of studies would allow for better understanding of the musculoskeletal abnormalities which may assist in finding an appropriate treatment.

Lastly, as mentioned before, AAV-gene therapy ICV-THAL treatment has greatly attenuated CNS signs; however, peripheral disease still exists. Therefore, treatment studies to target peripheral disease are needed to improve the quality of life of affected research animals and eventually, human patients.

References

Berns, K. (1990). Parvovirus replication. *Microbiological reviews* , 316-329.

Bley, A.G., *et al* (2011). Natural history of infantile GM2 gangliosidosis. *Pediatrics* , e1233-e1241.

Blood, D.C., *et al* (1999). *Sauders Comprehensive Veterinary Dictionary.* London: Elsevier.

Bradbury, A.M., *et al* (2009). Neurodegenerative lysosomal storay disease in European Burmese cats with hexosaminidase beta-subunit deficiency. *Molecular Genetics and Metabolism* , 53-59.

Cork, L.M., *et al* (1978). The Pathology of Feline GM2 Gangliosidosis. *American Journal of Pathology* , 723-730.

Evans, H. (1993). *Miller's Anatomy of the Dog.* Phildelphia: Elsevier.

Federico, A.P., *et al* (1991). The clinical aspects of adult hexosaminidase deficiencies. *Developmental neuroscience* , 280-287.

Fuller, M.M., *et al* (2006). Epidemiology of lysosomal storage diseases: an overview. *Oxford PharmaGenesis* , Chapter 2.

Lin, H.S., *et al* (2013). Assessment of bone mineral density by dual energy x-ray absorptiometry in patients with mucopolysaccharidoses. *Orphanet Journal of Rare Diseases* , 71.

Liu, Y.H., *et al* (1997). Mouse model of GM2 activator deficiency manifests cerebellar pathology and motor impairment. *Proceedings of the National Academy of Sciences* , 8138-8143.

Maegawa, G.S., *et al* (2006). The natural history of juvenile or subacture GM2 gangliosidosis: 21 new cases and literature review of 134 previously reported. *Pediatrics* , e1550-e1562.

Martiniuk, F.C., *et al* (1998). Carrier frequency for glycogen storage disease type II in New York and estimates of affected individuals born with the disease. *American Journal of Medical Genetics* , 69-72.

Porter, B.L., *et al* (2011). Pathology of GM2 gangliosidosis in Jacob sheep. *Veterinary Pathology* , 807-813.

Rabinowitz, J.S., *et al* (2000). Building a better vector: the manipulation of AAV virions. *Virology* , 301-308.

Rossi, L.Z., *et al* (2011). Bone involvement as presenting sign of pediatric-onset Gaucher disease. *Joint Bone Spine* , 70-74.

Sandhoff, K. (2013). Metabolic and cellular bases of sphingolipidoses. *Biochemical Society Translation* , 1562-1568.

Torres, P.Z., *et al* (2010). Tay-Sachs disease in Jacob sheep. *Molecular Genetics and Metabolism* , 357-363.

Vite, C.P., *et al* (2003). Adeno-associated virus vector-mediated transduction in the cat brain. *Gene Therapy* , 1874-1881.

Wasserstein, M.G., *et al* (2012). Skeletal manifestations in pediatric and adult patients with Niemann Pick disease type B. *Journal of Inherited Metabolic Disease* , 123-127.

White, K. (2011). Orthopaedic aspects of mucopolysaccharidoses. *Rheumatology* , 26-33.

Xing, E.M., *et al* (2013). The effect of neonatal gene therapy on skeletal manifestations in mucopolysaccharidosis VII dogs after a decade. *Molecular Genetics and Metabolism* , 183-193.

Zar, J. (1984). *Biostatistical Analysis, Second Edition.* Englewood Cliffs, NJ: Prentice-Hall.

Appendix

Micro-CT Analysis of Limb Bones

Introduction

Limb samples of GM2 immature and GM2+AAV and normal/carrier sex/age-matched control subjects taken at necropsy were sent to the McNulty Lab at Louisiana State University School of Veterinary Medicine (Baton Rouge, LA) for Micro- (μ) CT analysis. μCT functions virtually the same as conventional CT as explained previously. However, μCT scans samples of much smaller size but at a much higher resolution. Higher resolution allows detection of differences in bony make-up (cortical, trabecular, etc) that are not detectable on conventional CT images. Although vast bony changes were observed and quantified using conventional CT, our goal in submitting samples for μCT was to detect and quantify the differences in bone turnover of GM2 cats with skeletal abnormalities as compared to controls.

Materials and Methods

Thoracic and pelvic limbs were sent for μCT analysis from four GM2+AAV cats with one female GM1 carrier control and 3 GM2 immature cats with two normal female controls. Dr. Margaret McNulty analyzed the following samples: proximal, midshaft, and distal femur; proximal tibia; proximal humerus; and intact elbow joints. These sites were selected based on lesions seen previously on radiograph and CT images.

Samples from each subject were immersed in 70% ethanol (for density and bone volume parameters) and placed in holders for scanning in the Scanco μCT (Model 40; Scanco Medical AG, Basserdorf, Switzerland). Samples were scanned at 55kV with a 0.3 second integration time in a 30μm voxel size in a plane at 30μm slice thickness. The regions of interest (ROI) are as follows: distal 30% of femur to distal diaphysis for trabecular bone, and 50% of femoral length for midshaft femur for analysis of cortical bone; proximal 30% of humerus, and 50% humoral length for trabecular and cortical bone, respectively; proximal tibiae to distal tibial tuberosity, and lastly, distal 25% of humerus and proximal 25% of radius and ulna for elbow joint analysis. The following parameters were measured for trabecular and cortical bone: bone volume (BV), total volume (TV), BV/TV, tissue density (TD), apparent density (AD), trabecular number (TN), trabecular thickness (TT), connectivity density, (CD), and structural model index (SMI). Cortical bone was measured for cortical area (CA), cortical thickness (CK), and porosity (P). *See definitions on page 62.*

Results

Results were consistent with abnormalities observed on conventional CT images. GM2+AAV cats ranging from 17-30 months in age demonstrated a roughend articular surface of bone, with the oldest cat in the group exhibiting significant periarticular osteophyte formation on the medial surface of the distal femur as well as subchondral bone cyst formation (Figure A1). Additionally, fewer trabeculae and irregular cortical bone was present in GM2+AAV cats than normal controls (Figure A2).

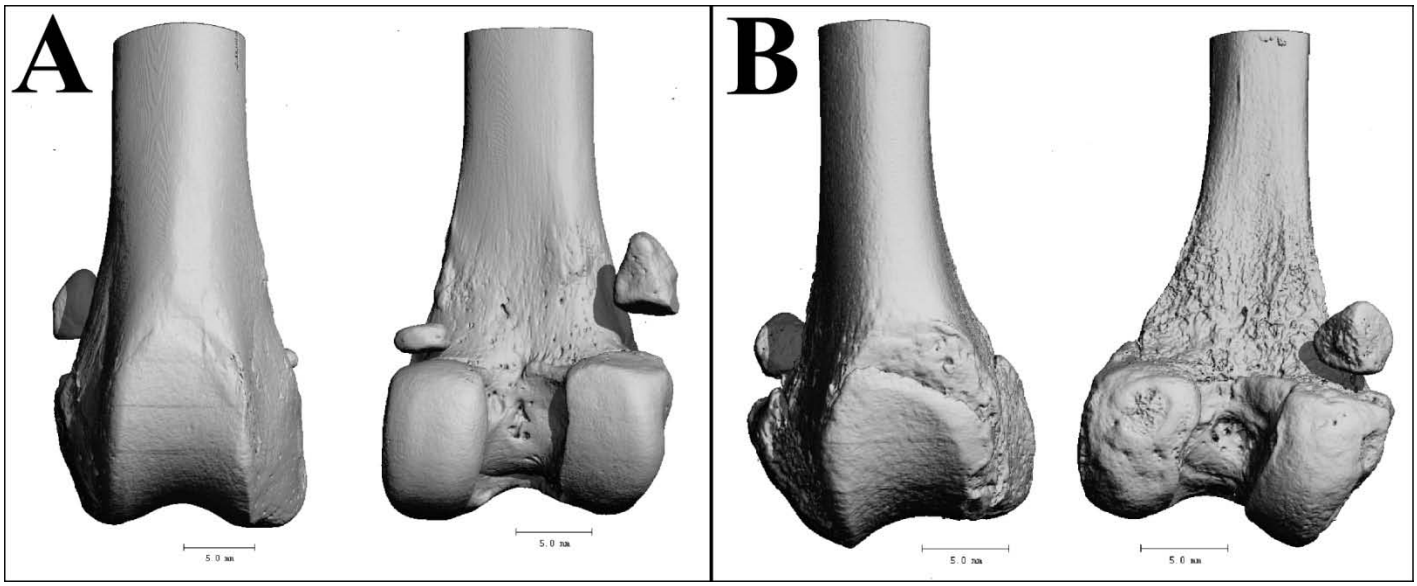

Figure A1: 3D reconstruction of µCT image of mature distal femora. (A): Cranial (left) and caudal (right) view of mature normal control. (B): GM2+AAV cat in same orientation as A. Note roughened articular surfaces, abnormally shaped fabellar sesamoid bone, and subchondral bone lesion on medial condyle compared to normal.

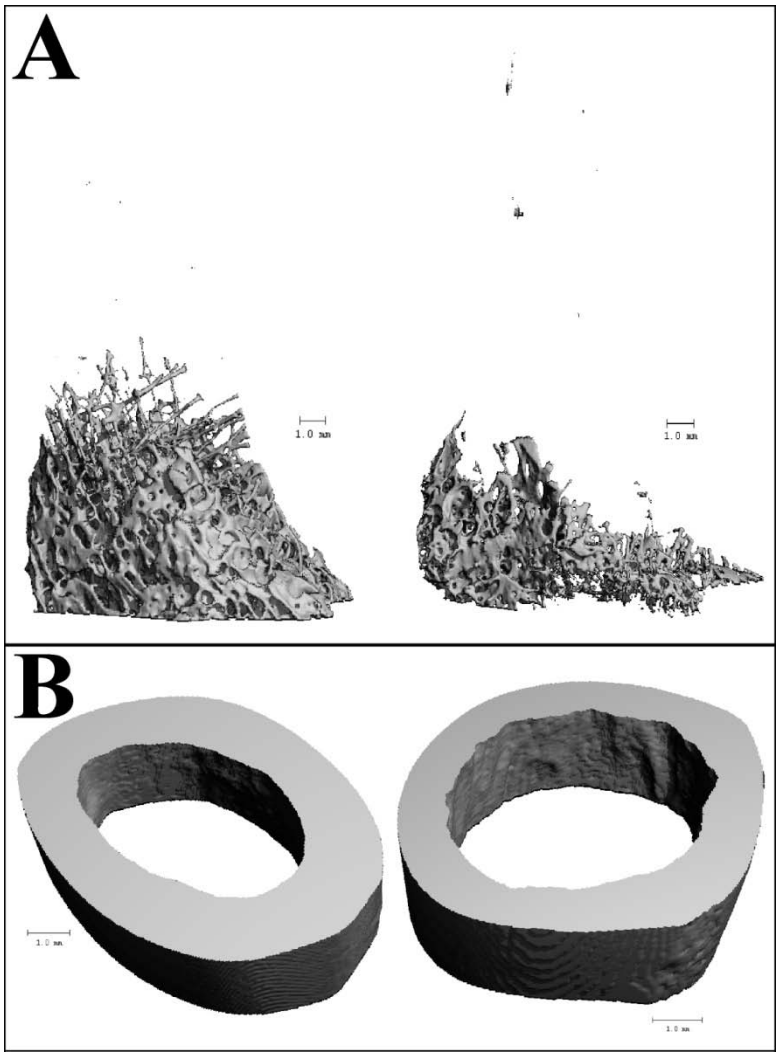

Figure A2: 3D reconstruction of μCT mature images. (A): Representation of trabecular bone of normal control (left) and GM2+AAV (right). Note the overall decrease in trabecular bone in the affected. (B): Representation of cortical bone with the same orientation. Note the irregularity of cortical bone in the affected (right) compared to normal (left).

Due to known effects of age on bone, groups for statistical analyses were created based on age, and additional samples were included in the present project to ensure adequate sample sizes for analyses (Table A1).

Table A1: µ-CT Measurements

		µ-CT Measurements							
A		**Humerus**							
GM2 Immature		**BV**	**BV/TV**	**CD**	**SMI**	**Mean**	**BS**	**BS/BV**	**DA**
7-1010		22.11	0.06	5.03	2.82	0.65	527.21	26.43	1.90
7-1006		16.18	0.05	4.21	3.07	0.67	419.72	29.92	1.68
Normal Immature									
11-1015		61.66	0.09	10.82	2.70	0.75	1453.97	25.69	1.80
9-1669		65.76	0.11	14.17	2.40	0.79	1447.12	23.46	1.71
9-1667		69.69	0.13	15.86	2.24	0.81	1523.76	23.07	1.78
GM2 + AAV Mature									
11-900		7.82	0.03	2.26	2.02	0.69	167.17	22.81	1.46
7-943		19.82	0.04	1.20	2.22	0.67	328.15	17.30	1.49
Normal Mature									
9-1594		65.79	0.10	1.80	1.50	0.75	829.47	12.73	1.65
7-758		94.11	0.07	2.24	1.40	0.66	1507.12	16.11	1.68

		µ-CT Measurements							
B		**Femur**							
GM2 Immature		**BV**	**BV/TV**	**CD**	**SMI**	**TN**	**TS**	**BS**	**BS/BV**
7-1010		12.25	0.03	2.09	2.71	0.27	3.74	270.90	24.39
7-1006		15.48	0.04	3.53	2.76	0.29	3.48	353.50	25.51
Normal Immature									
11-1015		90.15	0.16	18.57	2.09	0.54	2.07	1819.55	21.01
9-1669		95.28	0.21	18.77	1.46	0.64	1.85	1511.42	16.05
GM2 + AAV Mature									
11-900		24.77	0.07	3.96	1.90	0.36	2.87	425.48	17.75
7-943		22.00	0.03	1.35	2.22	0.20	5.03	440.25	20.92
Normal Mature									
9-1594		67.08	0.11	2.28	0.63	0.35	3.20	840.98	12.53
7-758		94.91	0.07	2.86	1.23	0.24	4.38	1678.93	17.73

Table A1: A. Humerus; B. Femur. Please refer to definitions on pages 64-65 for parameter explanation.

Upon trabecular analysis of femoral samples, it was found that both GM2 immature and treated cats exhibited a lower BV/TV ratio compared to controls. GM2+AAV cats had significantly lower BV compared to the normal control ($p=0.013$). GM2 immature cats were significantly different than normal in BV ($p=0.0015$) and BV/TV ($p=0.03$). GM2 immature cats also showed significantly lower bone surface ($p=0.014$) and persistant physes compared to controls (Figure A3).GM2+AAV cats exhibited more plate-like trabeculae than unaffected controls ($p=0.031$.) With respect to femoral samples, no other parameters reached significance between GM2+AAV and controls; however, CD was significantly lower in GM2 immature samples ($p=0.002$). GM2 immature cats also had fewer trabeculae ($p=0.028$) that were spaced significantly further than normal controls ($p=0.010$). Lastly, GM2 immature femoral CK was signficantly thinner than controls ($p=0.043$) (Figure A4).

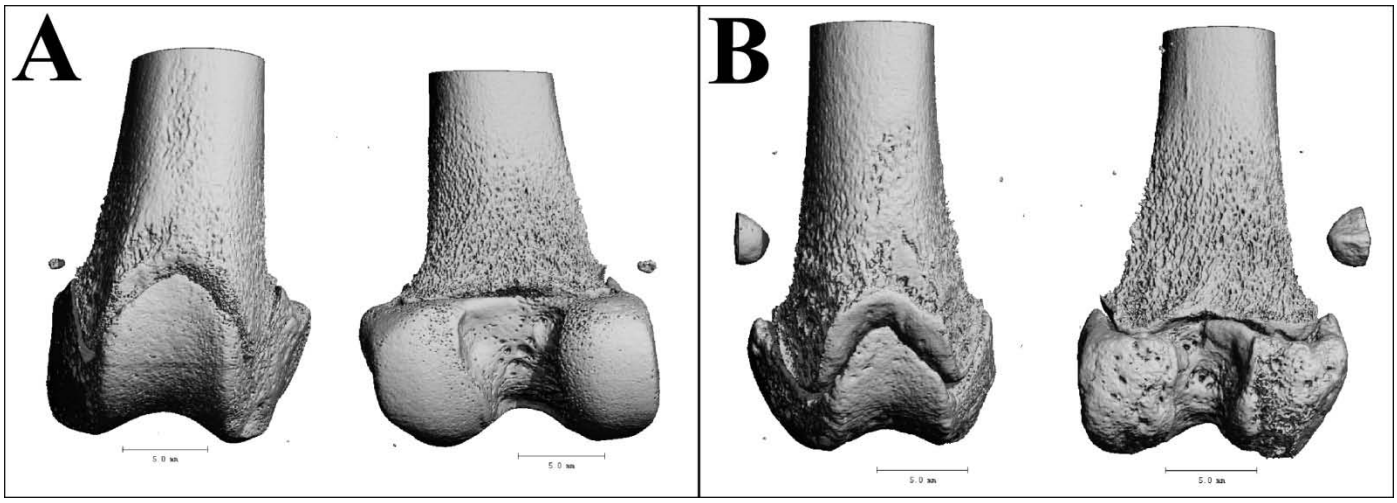

Figure A3: 3D reconstruction of µCT images of immature distal femora. (A) Cranial (left) and caudal (right) views of sex/age-matched control. (B) GM2 immature cat with the same orientation. Note the large underdeveloped physes and roughened condyles compared to (A).

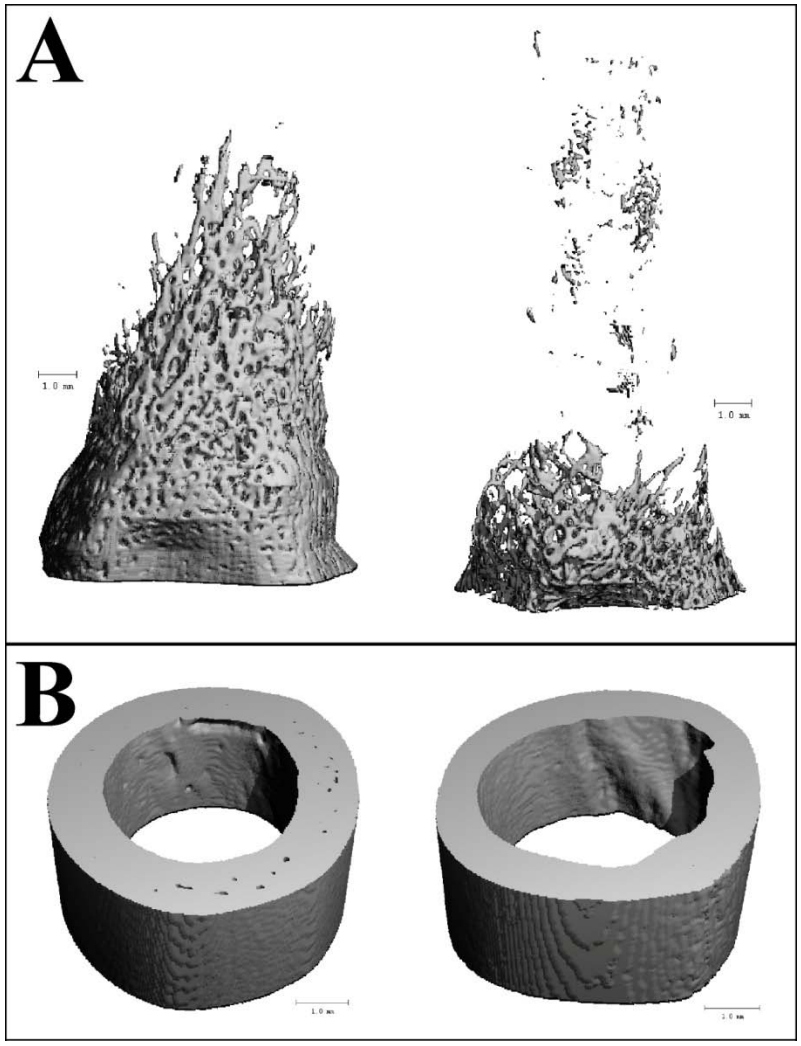

Figure A4: 3D reconstruction of µCT immature images. (A) Trabecular bone from a normal (left) and GM2 immature (right). Note the irregular dispersal and overall fewer trabeculae compared to normal. (B) Cortical bone in same orientation. Note the irregularity in GM2 immature compared to normal.

Humeral analyses were similar to femoral analyses in that GM2+AAV showed significantly lower BV ($p=0.05$) compared to normal controls as well as a higher plate-like trabeculae count ($p=0.0288$). GM2 immature cats demonstrated lower BV ($p=0.023$) and lower TV ($p=0.001$) as compared to unaffected. CD and TD were both significantly lower ($p=0.019$ and $p=0.014$, respectively) in GM2 immature cats compared to normal controls. Lastly, bone surface was lower in untreated ($p=0.0003$) than control, all of which were consistent with femoral measurements.

Discussion and Conclusions

Gross observation of femoral and humeral µCT samples are consistent with bony abnormalities observed on conventional CT. Additionally, statistical results of long bones further the findings on length measurement in GM2 immature and treated animals in that long bones are shortened in GM2 cats compared to controls, with the exception of femoral lengths that are normalized in GM2+AAV cats. This finding is consistent with the data showing untreated cats have significantly lower bone surface than control cats, a finding not seen in treated cats. Also, the more rigid plate-like trabeculae found in GM2+AAV when compared to normal may be due to compensation for the overall reduction in BV/TV in GM2+AAV as compared to normal.

We can conclude from this study that findings are consistent between both coventional CT and µCT, and that all GM2 cats demonstrate skeletal malformations. Although more research is needed, it can be inferred that while treatment is not stopping it, the progression of skeletal deformities may be slowing. Another hypothesis is that bone growth is simply retarded in GM2

cats, furthered by the persistent physes in GM2 immature cats. Because GM2+AAV cats live longer, they are able to reach a more mature bone growth, although smaller in stature than normal. Future research will attempt to determine if progression can be slowed further to delay or prevent potentially painful skeletal lesions such as periarticular osteophytes and roughened articular surfaces found in the mature GM2+AAV cat.

Future Studies

Elbow joints have been scanned but analyses are pending. After those analyses are conducted the McNulty lab aims to analyze lumbar vertebrae (irregular bones) and scapulae (flat bones) to determine if abnormalities persist in bones with different developmental processes. Lastly, histology of distal femora will investigate differences in osteoblasts and osteoclasts.

Limitations

Although we do see changes on conventional CT of lumbar vertebrae in GM2 animals compared to normal controls, cervical vertebrae are the most severely affected with respect to the spinal column. It is not possible to leave the cervical spine intact without compromising the integrity of the spinal cord at necropsy; therefore, we have been unable to prepare samples for µCT evaluation.

Acknowlegements

All measurements on the µCT work were done by Dr. Margaret McNulty and her lab at Louisiana State University School of Veterinary Medicine. All µCT figures courtesy of Dr.

Margaret McNulty. Thank you Dr. McNulty *et al* for conducting superior research on a novel topic and doing so in a prompt manner. Without your hardwork and passion for bone research, this project would have been missing an integral element, which has led to a strong collaboration that will truly help further the research to not only improve the quality of life for GM2 cats but also, eventually humans affected with this devastating disease.

μCT Definitions

Bone Volume (BV): the amount of bone (measured in $mm^{3)}$ in a region of interest (ROI).

Total Volume (TV): total volume of any ROI, including tissue.

Bone Volume/Total Volume (BV/TV): measured as a percentage by dividing the previous parameters, and used to normalize values.

Bone Surface (BS): surface of bone (measured in mm^2)

Degree of Anisotropy (DA): radius maximum and minimum of mean bone length.

Trabecular Number (TN): the number of trabeculae in any given ROI, measured in 1/mm.

Trabecular Spacing (TS): the distance between trabeculae, measured in mm.

Trabecular Thickness (TT): the diameter of trabeculae, measured in mm.

Tissue Density (TD): average density of everything in a ROI. (unit of hydroxyapatite density)

Apparent Density (AD): average density taken from tissue density that selects only for bone. (unit of hydroxyapatite density)

Cortical Area (CA): 2D measurement of cortical bone area.

Cortical Thickness (CK): average of thickness of cortical bone.

Cortical Porosity (CP): the porosity of cortical bone which is essentially solid; therefore, measured by 100-BV/TV.